THE OLIGOMERIC STATE OF ARCHAEAL FIBRILLARIN: IMPLICATIONS IN THE ORGANIZATION AND FUNCTION OF ESSENTIAL BOX C/D sRNP PARTICLES

PAULA LOUISE BURKE
Bachelor of Science, University of Lethbridge, 2003

A Thesis
Submitted to the School of Graduate Studies
of the University of Lethbridge
in Partial Fulfillment of the
Requirements for the Degree

MASTER of SCIENCE

Department of Chemistry and Biochemistry
University of Lethbridge
LETHBRIDGE, ALBERTA, CANADA

Abstract

Several vital cellular processes are preformed by large ribonucleoprotein (RNP) complexes. In archaeal and eukaryotic cells one example of these essential RNP particles is the box C/D sRNP. In archaea, this complex is responsible for methylation of ribosomal RNA (rRNA) and transfer RNA (tRNA) during their maturation. Archaeal fibrillarin (aFib) is the 2'-O methyltransferase responsible for catalysis by this complex. In this work we have identified the ability of aFib from *Sulfolobus acidocaldarius* to form dimers at biologically relevant concentrations and the structural determinants essential for this association. Based on our model we have predicted the ability of aFibs to form dimers in different archaeal and eukaryotic species. The ability of aFibs and their eukaryotic homologs to potentially adopt multiple conformations provides insight into the dynamics of the box C/D sRNP complex. As observed in the study of other essential RNP particles, the ability of these complexes to be conformationally diverse is integral to efficient catalysis of their varied substrates.

Table of Contents

Index of Tables

Index of Figures

List of Abbreviations

Ado-Met - S-adenosylmethionine
aFib – archaeal fibrillarin
aFib*Afu* – aFib from *Archaeoglobus fulgidus*
aFib*Mja* – aFib from *Methanococcus jannaschii*
aFib*Pfu* – aFib from *Pyrococcus furiosus*
aFib*Sac* – aFib from *Sulfolobus acidocaldarius*
$D_{w,20}$ – Diffusion coefficient for water at 20 °C
ΔH – change in enthalpy
GAR – glycine/arginine rich
IPTG – isopropyl-beta-D-thiogalactopyranoside
ITC – isothermal titration calorimetry
K^d – dissociation constant
mRNA – messenger RNA
M – molecular mass
PAGE – polyacrylamide gel electrophoresis
PCR – polymerase chain reaction
PFU – *Pyrococcus furiosus*
rmsd – root mean square deviation
RNP – ribonucleoprotein
rRNA – ribosomal RNA
$S_{w,20}$ – Sedimentation coefficient for water at 20 °C
SDS – sodium dodecyl sulfate
SEC – size exclusion chromatography
sRNA – sno-like or small RNA
snRNA – small nuclear RNA
snoRNA – small nucleolar RNA
TEMED – N,N,N',N'-tetramethyl-ethylenediamine
tRNA – transfer RNA

Chapter 1 - Background

1.1 - Ribonucleoprotein particles: A glimpse into the RNA world

Work performed in the last several decades has identified a number of essential ribonucleoprotein (RNP) complexes. These particles, comprised of one or more RNA molecules and associated proteins, are responsible for the most archaic cellular processes, including replication, post-transcriptional processing, transcript transport, cellular localization and production of nascent protein molecules (reviewed in Wassarman *et al*., 1999; Eddy, 2001; Erdmann *et al*., 2001). Discovery of these complexes, the elucidation of their integral functions and the ability of some RNA molecules to perform biochemical reactions has lead to the hypothesis that RNA was the precursor to DNA and proteins as the genetic storage and catalytic molecules, respectively, within the cell.

The most studied and well understood RNP is the ribosome, the cellular protein production machinery. Functional ribosomes result from the assembly of four different RNA molecules and 50 to 70 proteins. This large RNP complex adopts several well-defined conformations during its catalytic cycle and is essential for cell viability.

In general, RNP particles contain a relatively large number of components and are highly dynamic structures. Like the ribosome, other essential RNP particles including

telomerase (Beattie *et al*., 2001) and spliceosomes (reviewed by Jurica & Moore, 2003) adopt multiple conformations that modulate recognition and processivity. Knowledge of the stoichiometric composition and the multiple molecular conformations these complexes are likely to adopt provides insight into how they function. In this work we investigate the quaternary structure of archaeal fibrillarin (aFib) from *Sulfolobus acidocaldarius*. To function, aFib forms RNP assemblies with a box C/D small nucleolar (sno)-like or small RNA (sRNA) and two additional protein components, Nop5p and L7Ae. This complex is a simplified homolog to eukaryotic snoRNP particles, which methylate precursor ribosomal RNA (rRNA) and small nuclear RNA (snRNA) in sub-nuclear structures. In eukarya and archaea, Fib is the essential S-adenosylmethionine (Ado-Met)-dependent 2'-O methyltransferase responsible for RNA methylation (Wang *et al*., 2000; Omer *et al*., 2002).

1.2 - Cellular importance of RNA methylation in archaea

During the ribosomal maturation pathway, precursor rRNA transcripts are methylated by box C/D sRNP particles at 100 or more conserved sites within core regions of small and large subunit rRNAs (Maden, 1990; Lane *et al*., 1995). Methylation of RNA by box C/D sRNP particles results in the stabilization of both RNA-RNA and

RNA-protein interactions essential for ribosome assembly, structure and function. In particular, steric restrictions caused by 2'-O methyl groups results in a bias toward the C3'-endo ribose conformation, over the more common C2'-endo conformation (Voet & Voet, 2004). In purines and pyrimidines, the C3'-endo conformer (Figure 1; Kawai *et al*., 1992) stabilizes base stacking interactions and increases RNA helix rigidity (Davis *et al*., 1998). This conformational bias allows for formation of correctly folded rRNA structures which are further stabilized through the association of essential ribosomal proteins. In addition, methylation can protect RNA from degradation and increase hydrophobicity at RNA-protein contact surfaces, augmenting these interactions (Kowalak *et al*., 1994).

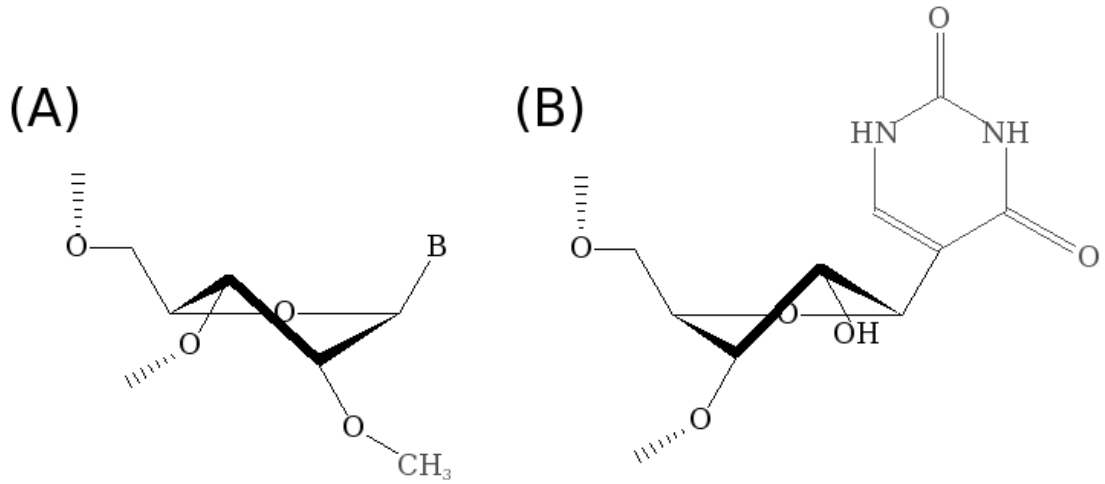

Figure 1: Major types of post-transcriptional RNA modifications (gray). (A) 2'-O methylated ribose in the C3' endo conformation (B) Isomerization of uridine to pseudouridine in the C2' endo conformation.

1.3 - The box C/D methylation complex

In archaea and eukarya two RNA families, C/D box and H/ACA box RNAs, are the guide components of RNP particles that perform the most common RNA modifications, 2'-O methylation and pseudouridylation respectively (Figure 1). These guide molecules are characterized by short, highly conserved 'box' sequences. Like their eukaryotic homologs, archaeal box C/D sRNAs can be identified by two sets of box C/D sequence motifs (Gaspin *et al*., 2000; Omer *et al*., 2000). The highly conserved C (RUGAUGA, where R represents a purine) and D (CUGA) box motifs are located at the 5' and 3' ends, respectively (Figure 2). The second, semi-conserved C' (UGAUGA) and D' (CUGA) box motifs are located internally, roughly 12 nucleotides from the terminal motifs (Cavaille and Bachellerie, 1998; Gaspin *et al*., 2000; Kiss, 2001; Tran *et al*., 2005). These conserved box C/D motifs form bipartite structures and are sites of protein assembly (Kuhn *et al*., 2002; Szewczak *et al*., 2002; Watkins *et al*., 2002).

The regions upstream of box D or D' motifs exhibit complementarity to sites of precursor rRNA and tRNA methylation (Figure 2). These anti-sense elements base pair with target RNA and direct ribose methylation five nucleotides upstream from the start of the D or D' motif; this is known as the 'N plus five' rule (Kiss-Laszlo *et al*., 1996; Tycowski *et al*, 1996). The RNA binding protein L7Ae is the first protein to interact

with the guide sRNA. This interaction occurs at the kink-turn (K-turn) conformation adopted by box C/D motifs (Watkins *et al*., 2000; Klein *et al*., 2001; Rozhdestvensky *et al*., 2003) and results in modified box C/D sRNA structure required for subsequent assembly (Cahill *et al*., 2002; Watkins *et al*., 2002; Moore *et al*., 2004; Suryadi *et al*., 2005). Interaction of aFib and Nop5p with box C/D sRNAs is not clearly understood. However, *in vitro* reconstitution of sRNP particles has demonstrated that L7Ae, Nop5p and aFib form identical protein complexes at both the C/D and C'/D' motif and interaction between these complexes is essential for efficient methylation of substrate RNA (Rashid *et al*., 2003; Tran *et al*., 2003).

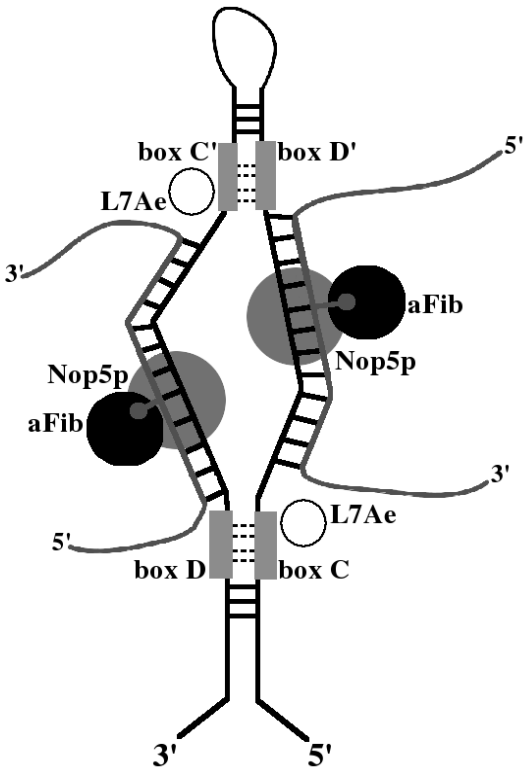

Figure 2: The minimal box C/D sRNP from archaea. Box C/D motifs are indicated by gray boxes. Target RNA is in duplex with guide sRNA and methyl groups indicated as circles (Based on figure in Clouet-d'Orval et al., 2005).

Archaeal and eukaryotic replication, transcription and translation systems are similar, in fact, the high similarity between these systems led to the separation of archaea and bacteria into unique domains. Consequently archaeal systems have been utilized to model equivalent eukaryotic systems that are more complex and difficult to study. Functional eukaryotic homologs for the archaeal box C/D sRNP components have been identified and are presented in Table 1 (Amiri, 1994; Gaspin *et al*., 2000; Kuhn *et al*., 2002; Omer *et al.*, 2000; Omer *et* al., 2003). Primary sequence alignments indicate the most divergent box C/D sRNP component is fibrillarin. In particular eukaryotic fibrillarins have an additional amino terminal glycine-arginine rich (GAR) domain in comparison with archaeal enzymes. The GAR domain is important for nucleolar localization in higher eukaryotes (Heine *et al*., 1993) but is not conserved in lower eukaryotes, or needed in archaea which do not form nucleoli. This suggests the GAR domain adds functionality to the common catalytic core and is not essential for catalysis. Therefore, work on the box C/D RNP components from archaea will increase our understanding of these essential complexes in both archaea and eukaryotes.

Table 1: Components of the homologous box C/D RNP complexes from archaea and eukarya.

Archaeal system	Eukaryotic homolog	Function
sRNA	snoRNA	guide RNA
aFib	Fib	methyltransferase
L7Ae	15.5 kDa protein	box C/D binding protein
Nop5p	Nop56 and Nop58	additional box C/D RNP proteins

Fundamental knowledge regarding the quaternary structures that box C/D RNP particles may form is important for understanding the function, regulation and dynamics of these structures. As evident from work performed thus far, our knowledge of these complexes at the molecular level is limited and incomplete. Due to its catalytic role and conflicting literature reports, the association of aFib in box C/D sRNP particles is of particular interest. In this study, a series of biochemical methods were employed to determine the oligomeric state of purified, recombinant aFib from *S. acidocaldarius* (aFib*Sac*). To determine whether aFib*Sac* forms amino termini mediated dimers, similar to those observed for aFib from *Methanococcus jannaschii (*Wang *et al*., 2000), a mutant lacking the amino terminal domain was generated and oligomeric state determined. Based upon these results we put forward a model that predicts the ability of aFib to form amino-terminus mediated dimers from primary sequence. We then test the model by constructing a mutant with an amino terminus predicted to form monomers in solution.

Chapter 2 - aFib*Sac* exists as an oligomeric mixture

2.1 - Introduction

Archaeal fibrillarin (aFib) is the catalytic component of an essential cellular RNP methylation complex that functions in rRNA and transfer RNA (tRNA) maturation. *In vitro*, aFib associates with Nop5p, L7Ae and one of many box C/D sRNAs to form functional complexes that transfer methyl groups to specific 2' hydroxyl groups of maturing rRNA and tRNA. Recent works have identified, to some extent, the architecture of the minimal box C/D RNP required for methylation in archaea (Omer *et al*., 2002; Aittaleb *et al*., 2003; Rozhdestvensky *et al*., 2003; Tran *et al*., 2003; Aittaleb *et al*., 2004; Moore *et al*., 2004) and eukaryotes (Cahill *et al*., 2002). However, many fundamental questions remain regarding the molecular events that are associated with function. These include basic biochemical information, such as the stoichiometric association of individual proteins within the functional sRNP complex in the absence and presence of substrate. Understanding these associations will provide insight into the interaction of sRNP molecules with different substrates and the nature of the likely interactions between independent box C/D RNP complexes.

aFibs are particularly interesting as conflicting evidence exists regarding their

oligomeric state (Wang *et al*., 2000; Aittaleb *et al*., 2003; Deng *et al*., 2004). The fibrillarin homolog from the hypothermophile *M. jannaschii* (aFib*Mja*) is a dimer in crystallographic space (Wang *et al*., 2000). The aFib*Mja* dimer has a buried surface area of 1700 $Å^2$, above the accepted value for a dimer of 1050 $Å^2$ (Chothia and Janin, 1975), and is non-monomeric on non-denaturing polyacrylamide gel electrophoresis (Wang *et al*., 2000). Conversely, fibrillarin homologs from *Archaeoglobus fulgidus* (aFib*Afu*) and *Pyrococcus furiosus* (aFib*Pfu*) are monomers in crystallographic space and elute from gel filtration columns at retention volumes corresponding to monomers (Aittaleb *et al*., 2003; Deng *et al*., 2004). While the oligomeric state does not appear to be essential for catalysis, the oligomeric state of aFibs will have functional consequences at the molecular level.

In order to understand the molecular properties of aFibs and sRNPs, a detailed analysis of aFib*Sac* oligomeric state has been completed using biochemical methods.

2.2 - Methodology

2.2.1 - Expression and purification of recombinant wildtype and 6x His tagged aFib*Sac:*

Escherichia coli strain BL21 (DE3)pLysS cells containing wildtype recombinant aFib*Sac* in a pET3d expression vector grown in Luria Bertani broth were inoculated with 1 mM isopropyl-beta-D-thiogalactopyranoside (IPTG) at optical densities between 0.5 and 0.7 at 600 nm. *E. coli* strain BL21 (DE3)pLysS cells containing aFibSac with an amino terminal 6x His tag (aFibSac_N23) in a pET28a expression vector were grown and inoculated with IPTG under conditions described above. Inoculated cells over expressed aFib*Sac* and aFib*Sac*_N23 overnight with shaking at 37 °C.

Cells over expressing aFib*Sac* were sonicated in buffer A (10 mM Tris-HCl (pH 8.5), 100 mM NaCl, 1 mM β-mercaptoethanol and 0.1 mM EDTA). After an initial centrifugation step at 14,000 rpm for 1 h, aFib*Sac* was purified from contaminants by incubation at 85°C for 4 minutes. Thermoprecipitation was followed by separation on a 24 mL size exclusion chromatography (SEC) column (Amersham Biosciences, Pittsburgh, PA, Superdex^{TM} 200) run at 4 °C in buffer B (10 mM KH^2PO^4 (pH 7.0), 100 mM NaCl, 1 mM β-mercaptoethanol and 0.1 mM EDTA) achieving approximately 97% purity.

Over expression of recombinant 6x His tagged aFib*Sac* lead to the production of

inclusion bodies. Therefore cells over expressing aFib*Sac*_N23 were sonicated under conditions that allowed the recombinant protein to solublize in buffer C (10 mM Tris-HCl (pH 8.5), 100 mM NaCl, 20% glycerol, 4 M urea) and centrifuged as described above. Thermoprecipitation could have been use to purify 6x His tagged mutants, however, elution from a Ni-NTA agarose (Qiagen, Hilden, Germany) efficiently produced samples of higher purity (~99%). aFib*Sac*_N23 was bound to a 3 mL Ni-NTA agarose column at room temperature, equilibrated with buffer C, to remove contaminants. Binding was followed by a wash step with buffer D (10 mM Tris-HCl (pH 8.0), 100 mM NaCl, 20% glycerol, 25 mM imidazole). Bound protein was eluted with buffer E (buffer D supplemented to 250 mM imidazole). The amino terminal 6x His tag of aFib*Sac*_N23 was removed at room temperature with 2.7 nM of thrombin. Thrombin cleavage results in the removal of seventeen amino acids, leaving a six residue addition at the amino terminus (aFib*Sac*_N6). Cleaved and uncleaved proteins were separated by a second run through a Ni-NTA column, at room temperature, equilibrated with buffer D and eluted with buffer E. Cleaved protein was then injected onto a SEC column equilibrated with buffer B as described above for wildtype aFib*Sac*. Tagged, cleaved and wildtype aFib*Sac* behaved similarly during resolution by both SDS-PAGE and SEC.

2.2.2 - Homology modeling and construction of aFib*Sac dimer model:*

Primary sequence identity of fibrillarin homologs aFib*Mja* and aFib*Sac* was determined to be 51% by **CLUSTALW** (Thompson *et al*., 1994). The solved three dimensional structure of aFib*Mja* (Wang *et al*., 2000; PDB: 1FBN) served as a template to generate a homology model of aFib*Sac* using **SWISS MODEL** (Schwede *et al*., 2003). Molecular superposition of the aFib*Sac* homology model and each aFib*Mja* subunit was performed with Swiss-Pdb Viewer (Guex & Peitsch, 1997) to generate a model of the aFib*Sac* dimer. Stereochemical properties of the modeled aFib*Sac* monomer were analyzed by **WHAT IF** and determined to be within acceptable limits for all parameters tested (Vriend, 1990).

2.2.3 - Size exclusion chromatography of wildtype aFib*Sac:*

aFibSac samples (300 mL) at 75.6 and 189.0 μM were injected onto a 24 mL SEC column (SuperdexTM 200) equilibrated at 4 °C with buffer B and run at 0.4 mL min-1. Apparent molecular weights were estimated by comparing the elution volume of aFibSac to a standard curve constructed using size exclusion protein standards (Amersham Biosciences, Pittsburgh, PA).

2.2.4 - Analytical ultracentrifugation of wildtype and 6x His tagged aFib*Sac:*

Sedimentation equilibrium experiments were performed on aFib*Sac* at 38.0, 49.5, and 75.6 μM in buffer F (25 mM Tris-HCl (pH 8.0), 100 mM NaCl). Sedimentation equilibrium experiments were conducted at 20 °C in a Beckman XL-I analytical ultracentrifuge using absorbance optics following standard procedures (Laue & Stafford, 1999). 110 ml aliquots of sample solution were loaded into 6-sector CFE sample cells, allowing the three concentrations to be run simultaneously. Runs were performed at 32,000 and 34,000 rpm. Each speed was maintained until no significant difference in $r^2/2$ versus absorbance was detected. Absorbance scans were taken at two hour intervals to ensure that equilibrium was achieved.

Sedimentation velocity experiments were performed on aFib*Sac*_N23 at 56.6 and 212.8 μM in buffer F. All experiments were conducted at 20 °C in a Beckman XL-I analytical ultracentrifuge using absorbance optics following standard procedures (Laue & Stafford, 1999). 400 mL aliquots of protein sample were loaded into 2-sector CFE sample cells and runs were performed at 50,000 rpm for approximately 3 h during which time a minimum of 50 scans were taken to monitor the sedimentation rate of the protein.

Experimental sedimentation coefficients ($S_{20,w}$) were determined using the program **SVEDBERG** (Philo, 1997), which incorporates a modified Fujita-MacCosham

function into a non-linear least squares fitting routine to fit the sedimentation boundaries to either single species or multiple species models. The program **SEDNTERP** was employed to calculate the partial specific volume of the protein (v), the solvent density (ρ) and viscosity using calculations detailed by Laue *et al.* (1991). Upon obtaining experimental values for $S_{20,w}$ and the diffusion coefficient ($D_{20,w}$), formula 1 was used to calculate molar masses (M).

$$M = \frac{s\,RT}{D\,(1 - v\rho)} \qquad \textbf{(Equation 1)}$$

M = molecular weight (Da), $S_{20,w}$ = sedimentation coefficient (Svedbergs), R = ideal gas constant (J mol^{-1} K^{-1}), T = temperature (K), $D_{20,w}$ = diffusion coefficient (cm^2 s^{-1}), v = partial specific volume of the protein (mL g^{-1}), ρ = the solvent density (g mL^{-1})

Experimental $S_{20,w}$ values were compared to theoretical hydrodynamic properties of a modeled aFib*Sac* monomer and dimer computed with the bead modeling software **HYDROPRO** (Garcia de la Torre *et al*., 2000).

2.2.5 - Isothermal titration calorimetry of wildtype aFib*Sac:*

Titration experiments were performed by isothermal titration calorimetry (ITC) using a VP-ITC microcalorimeter (Microcal LLC, Northampton, MA). All experiments were conducted at 30 °C with constant stirring (400 rpm) following standard procedures

(Beaudette & Langerman, 1978). The sample cell was loaded with 1.4 mL of protein in buffer B while the reference cell contained buffer B. Experiments included 20 to 30 equivalent injections of 5 mL of buffer A into the sample cell, followed by a 5 minute equilibration, while continuously monitoring the change in heat evolved. Proteins concentrations were determined by Bradford assay versus bovine serum albumin standards (Bradford, 1976). Differential power per second peaks were integrated using **ORIGIN** software (OriginLab Corp., Northampton, MA) and plotted versus protein concentrations in standard graphing software.

2.2.6 - Polyacrylamide gel electrophoresis of wildtype aFib*Sac:*

Sodium dodecyl sulfate-polyacrylamide gel electrophoresis (SDS-PAGE) was performed as described by Laemmli (1970) using a 4% polyacrylamide stacking gel and a 15% polyacrylamide resolving gel at 200 V in a vertical slab gel apparatus (Bio-Rad Laboratories Inc., Hercules, CA). The non-denaturing PAGE protocol was adapted from Reisfeld *et al*., (1962). All non-denaturing PAGE was performed with inverse polarity at 100 V in an acidic, β-alanine-acetate running buffer (140 mM β-alanine, 350 mM glacial acetic acid (pH 4.0)) at 4 °C. Resolving gels were prepared to pH 5.5 (15% acrylamide/bis-acrylamide, 375 mM sodium acetate (pH 5.5), 7 mM ammonium

persulfate, 0.05% N,N,N',N'-tetramethyl-ethylenediamine (TEMED)) and stacking gels were prepared to pH 6.8 (5% acrylamide/bis-acrylamide, 125 mM acetic acid/KOH (pH 6.8), 4 mM ammonium persulfate, 0.1% TEMED). Non-denaturing PAGE samples were loaded with a 5X sample buffer (310 mM TrisHCl (pH 6.8), 50% Glycerol, 0.03% methyl green). Protein bands on SDS and denaturing gels were visualized with Coomassie brilliant blue R-250 stain and compared to low molecular weight standards (Bio-Rad Laboratories Inc., Hercules, CA).

2.3 - Results

2.3.1 - Size exclusion chromatography analysis of wildtype aFib*Sac:*

In order to characterize the quaternary structure of aFib*Sac*, purified samples were separated by SEC under native conditions. Initial SEC experiments on aFib*Sac*, at 75.6 μM, produces a bimodal chromatogram with a primary peak centered at a retention volume of 15.62 mL and a secondary peak at 14.25 mL (Figure 3, dashed trace). Elution peaks at 14.25 mL and 15.62 mL correspond to apparent molecular weights of 77.8 and 38.2 kDa, respectively. The sequence predicted molecular weight of monomeric aFib*Sac* is 26.5 kDa, in the absence of solvent, and 53.0 kDa for the corresponding dimer.

Discrepancies observed between molecular weight estimations by SEC and from sequence likely result from at least three sources: (1) SEC elution volumes depend upon

the hydrated radii of the molecule, (2) SEC assumes all molecules are spherical and (3) broad peaks may overlap resulting in perturbed elution volumes. Inspection of the modeled aFib*Sac* dimer shows this structure is an elongated ellipsoid, not a symmetrical sphere. Therefore, all three mechanisms, asymmetry, solvation and peak overlaps (Figure 3), give rise to the differences in SEC estimated and theoretical molecular weights.

As the aFib*Sac* concentration was increased to 189.0 μM a similar bimodal chromatogram was observed (Figure 3, solid trace). The peak height ratio from chromatograms at 75.6 μM is 0.4, calculated as secondary peak A^{280} signal divided by primary peak A^{280} signal (S peak / P peak). However, the peak height ratio at 189.0 μM shifts to 0.7, suggesting a greater fraction of the higher molecular weight species. In addition to monomeric and dimeric elution peaks, at loading concentrations equal to or higher than 300 μM, chromatograms of purified aFib*Sac* exhibit a concentration dependent peak at void volumes (data not shown) indicating that much higher order oligomers are forming, although we do not know if these represent specific or functionally relevant aggregates. Equilibration of aggregate formation was sufficiently slow, relative to the duration of the separation, such that monomeric, dimeric and aggregate forms of aFib*Sac* could be clearly resolved as distinct peaks in the elution

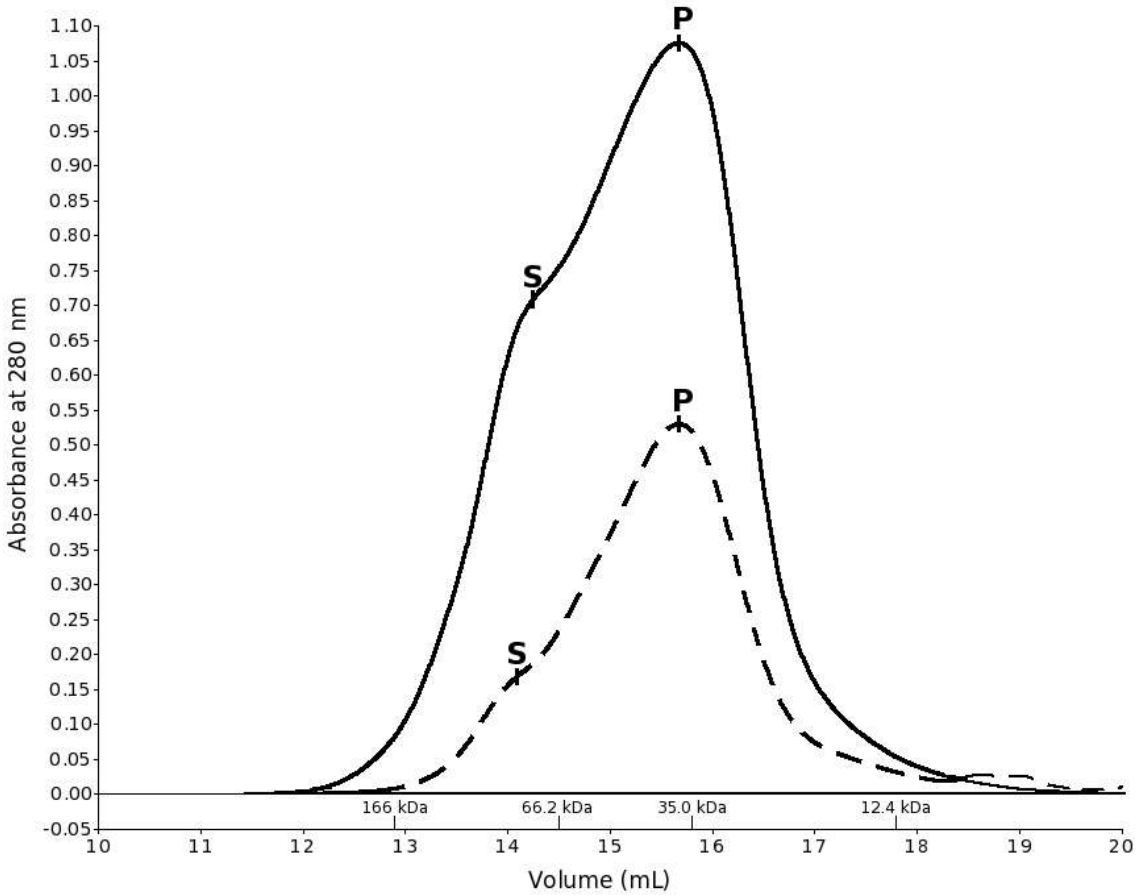

Figure 3: Size exclusion chromatography of aFib*Sac showing the UV absorbance at 280 nm as a function of elution volume. Equivalent volumes (400 μL) of* aFib*Sac at 75.6 (dashed line) and 189.0 μM (solid line) were run on a SuperdexTM 200 column. Elution volumes of protein standards are marked along the volume axis and corresponding molecular weights noted above. Primary and secondary peaks are indicated by the letters "P" and "S" respectively. Absorbance at 280 nm is a logarithmic measure of optical density.*

profiles of high concentration samples. At very low concentrations a single peak centered at a retention volume corresponding to an aFib*Sac* monomer was observable (data not shown). Conversely, a single peak at retention volumes corresponding to a dimer was not observed.

The absence of a single dimer peak is likely due to dilution of sample as it

progresses with the mobile phase. Dilution of protein samples on SEC columns results from diffusion of protein along the gel bed and/or interaction of protein molecules with the column matrix. Either mechanism results in a broadening of elution peaks and dilution of sample. For concentration dependent complexes this dilution can result in dissociation of the complex if the resulting concentration is below that required for association. This may explain the bimodal peaks that were consistently observed on chromatograms of purified aFib*Sac* regardless of load concentration.

By SEC, three distinct molecular weight species were observed that indicate monomeric, dimeric and higher order oligomers, exist and are related in a concentration dependent manner. However, aFib*Sac* does not elute as a singular oligomeric species by SEC. In order to further characterize the oligomeric state of aFib*Sac* under native-like conditions a complementary technique, analytical ultracentrifugation, was also used.

2.3.2 - Analytical ultracentrifugation experiments on 6x His tagged aFib*Sac at varying concentrations:*

SEC experiments under native conditions suggest aFib*Sac* exists as an oligomeric mixture of monomers and dimers. The association of aFib*Sac* monomers into dimers is concentration dependent and dilution, for reasons discussed above (2.3.1), does not produce a singular dimer peak. Sedimentation velocity studies at 56.6 and 212.8 μM,

were employed to confirm and complement the SEC data.

At low aFib*Sac*_N23 concentrations the experimentally determined $\boldsymbol{S_{20,w}}$ and $\boldsymbol{D_{20,w}}$ are 2.759 S and 10.82 x 10^{-7} cm^2 s^{-1} respectively. The experimentally determined values are in good agreement with theoretical $\boldsymbol{S_{20,w}}$ and $\boldsymbol{D_{20,w}}$, 2.792 S and 8.626 x 10^{-7} cm^2 s^{-1} respectively, calculated by **HYDROPRO**. At this concentration, the experimental $\boldsymbol{S_{20,w}}$ and $\boldsymbol{D_{20,w}}$ correspond to a calculated apparent molecular weight of 24.3 kDa (as calculated by Equation 1) and is consistent with aFib*Sac*_N23 existing as a monomer (28.9 kDa).

At higher concentrations, sedimentation of aFib*Sac* proceeds faster ($\boldsymbol{S_{20,w}}$ = 3.208 S), indicating it is larger than aFib*Sac* at low concentrations, and the data fits a single species model. This suggests that at high concentrations the larger molecular weight sample is largely homogeneous. The $\boldsymbol{D_{20,w}}$ determined at this loading concentration was significantly over estimated (21.03 x10^{-7} cm^2 s^{-1}), as compared to theoretical values (6.273 x 10^{-7} cm^2 s^{-1}), resulting in a calculated molecular weight (14.3 kDa) much lower than the sequence predicted molecular weight of 52.8 kDa. Over estimation of translational diffusion is characteristic of a conformationally heterogeneous sample, which is consistent with our SEC data at high concentrations, treated under a single species model (Philo, 1994).

Moving boundary sedimentation, or sedimentation equilibrium, can be used to

obtain correct quantities and hydrodynamic properties of macromolecules in multiple component systems. However, in order to resolve the sedimentation boundaries of each component by sedimentation equilibrium the system must achieve and retain equilibrium at experimental speeds.

Sedimentation equilibration experiments of aFib*Sac* resulted in rapid aggregation in the sample cell and unresolvable sedimentation boundaries suggesting aFib*Sac* oligomerization is a slow, reversible, self aggregating system (Schachman & Harrington, 1954; Hersh & Schachman, 1955) making this system unsuitable for sedimentation equilibrium experiments (Kegeles, 1972). Interestingly, a self aggregating system is consistent with the concentration dependent aggregate peaks observed at flow through volumes in SEC experiments.

Without an accurate diffusion coefficient, which provides information about size, shape and hydration of a macromolecule, molecular weight cannot be correctly calculated. However, treatment of multiple component sedimentation velocity data under a single species model does give a relatively accurate sedimentation coefficient for the predominant species (Philo, 1994). Using the experimentally determined $\boldsymbol{S_{20,w}}$ (3.208 S) and the theoretical $\boldsymbol{D_{20,w}}$ computed for the modeled dimer (6.273×10^{-7} cm^2 s^{-1}), the calculated molecular weight (Equation 1) of the predominant species at this concentration

is 48.9 kDa, indicating an aFib*Sac* dimer, almost exactly double the observed molecular weight at low aFib*Sac* concentrations.

2.3.3 - Isothermal titration calorimetry studies of wildtype aFib*Sac association:*

Having shown the presence of monomers and dimers by SEC and analytical ultracentrifugation, the dimerization constant was determined by ITC. The enthalpy change (ΔH) associated with conformational changes in aFib*Sac* was determined by ITC in the concentration range 211 to 38.7 μM. ΔH is a constant between 211 and 63.6 μM and between 60.3 and 38.7 μM. As seen in Figure 4, ΔH undergoes a sigmoidal transition between 63.6 and 60.3 μM indicating aFib*Sac* is undergoing a specific change in conformational state. The dissociation constant (K^d) for this transition is 61.9 μM (Figure 4). Given the previously discussed SEC and analytical ultracentrifugation results, we propose this change results from a change in the oligomeric state of aFib*Sac* from dimer to monomer.

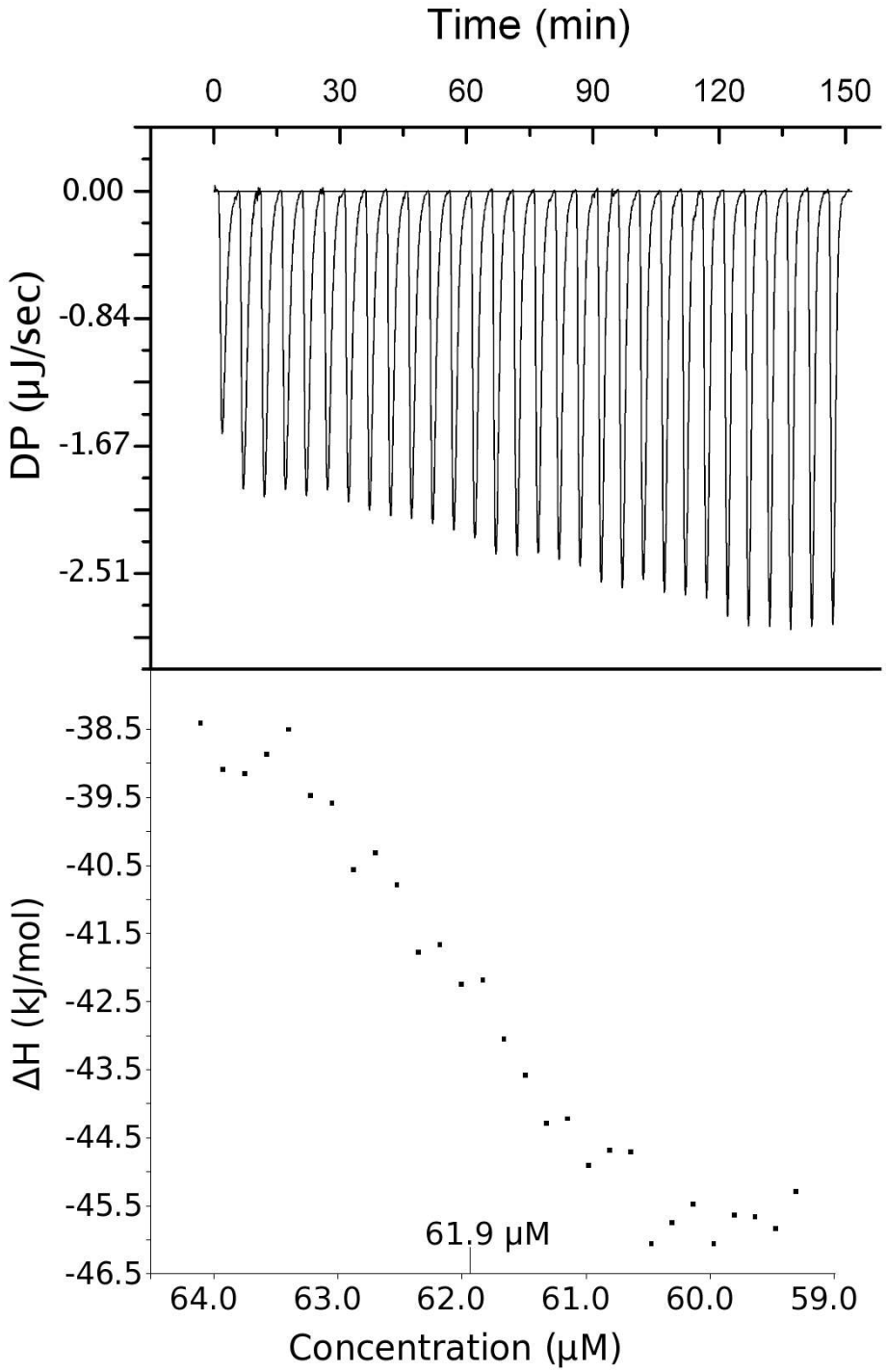

Figure 4: Differential power as a function of time data obtained for injections of buffer into aFibSac protein solution at 64.3 µM (upper panel). The enthalpy of association of aFibSac as a function of concentration as determined by ITC at 30°C (lower panel). The association constant for this transition is 61.9 µM and most likely corresponds to the monomer to dimer transition.

2.3.4 - Polyacrylamide gel electrophoresis analysis of aFib*Sac:*

As seen in Figure 5A purified aFib*Sac* (26.4 kDa) behaves anomalously under standard SDS-PAGE conditions. Anomalous migration on SDS-PAGE can be attributed to post-translational modifications (Marciani & Papamatheakis, 1978; Billings *et al*., 1979), excess positive or negative charges (Armstrong & Roman, 1993; Hu & Ghabrial, 1995), and hydrophobicity (Hu & Ghabrial, 1995). These characteristics largely result in bands that migrate at rates which cause over or under estimation in molecular weight, however, aFib*Sac* produces multiple bands with apparent molecular weights that are consistent with the presence of monomers, dimers and higher order oligomers. Amino terminal sequencing of higher order bands shows these are, in fact, aFib*Sac* and not residual impurities from purification (Personal communication, Dr. Steven Mosimann). The appearance of the SDS resistant oligomers appears to be concentration dependent as seen in lanes 1 and 2 (Figure 5A). A 10 fold excess of SDS in the sample reducing buffer reverses the oligomerization and aFib*Sac* migrates largely as a single band of expected molecular weight (lane 3). The reversible nature of oligomers formed at high concentration suggest aFib*Sac* is not completely denatured under standard SDS-PAGE conditions. Further, it demonstrates aFib*Sac* oligomers do not result from covalent attachment of subunits.

SDS stable dimers have been observed in other protein systems and have been inferred to be biologically important (LaDu *et al*., 1995; Ettinger *et al*., 1998; Gentile *et al*., 2002). Of particular interest are the SDS-resistant dimers of β-glycosidase from an extreme thermophile, *Sulfolobus solfataricus* (Gentile *et al*., 2002). Through a series of dynamic molecular modeling experiments Gentile and coworkers (2002) showed that intermolecular ionic and hydrogen bonding interactions increased as a function of temperature and SDS concentration due to desolvation of the protein surface. Due to the extreme thermophilic nature of *S. acidocaldarius* similar rationale can be applied to the observance of SDS-stable oligomers of aFib*Sac*, especially in the presence of heat.

The high isoelectric point of aFib*Sac*, 8.31 (Gasteiger *et al*., 2005), required a modified non-denaturing PAGE protocol to visualize aFib*Sac* under non-denaturing conditions. A aFib*Sac* oligomer distribution similar to that observed for SDS-PAGE was resolved by non-denaturing PAGE (Figure 5B), supporting results obtained by SEC and analytical ultracentrifugation. However, because of decreased aFib*Sac* solubility in acidic conditions, a light protein precipitate was observed in the loading wells, due to acidity of the running buffer, limiting the reliability of these results.

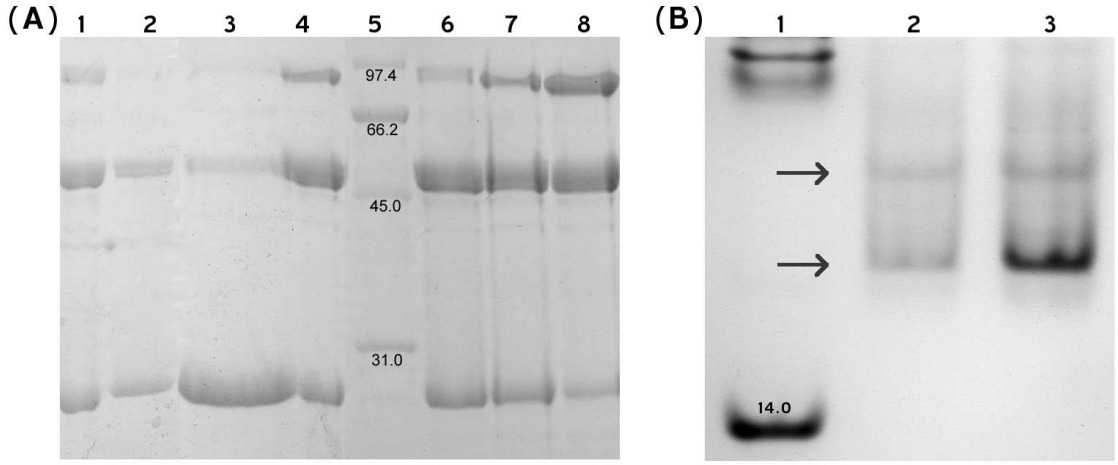

Figure 5: (A) 15% SDS-PAGE of purified aFib*Sac as a function of sample preparation. In lanes 1 and 2, 10 μL of 80.0 and 20.0 μM sample were loaded without exposure to heat. 5 μL of 160.0 μM sample was loaded in the presence of a 10 fold excess of SDS (lane 3) and under standard conditions (lane 4) without exposure to heat. Lane 5 contains 1 μL of low molecular weight marker. Lanes 6-8 contain 10 μL of 40.0 μM sample, with a 5 min heat step at 85 °C and with a 10 min heat step at 85 °C. (B) 15% non-denaturing PAGE of purified* aFib*Sac. Lane 1 contains 5 μL of low molecular weight marker. In lanes 2 and 3, 20 μL of 80 and 120 μM sample were loaded respectively. Two molecular weight species were resolved and are indicated by arrows.*

2.4 - Discussion

To date, characterization of box C/D sRNP associated proteins has identified two key interactions, the formation of an aFib/Nop5p heterodimer and interaction of L7Ae with guide sRNA, which have lead to the construction of a model of the minimal box C/D sRNP complex (Figure 6B) (Aittaleb *et al*., 2003; Fatica & Tollervey, 2003). In addition to interactions within sRNP particles, data in the literature suggests interactions between independent sRNPs supporting the existence of oligomeric sRNP complexes. In this work, a series of biophysical techniques have been utilized to demonstrate that purified aFib from *S. acidocaldarius* forms oligomers with a dissociation constant of 61.9 μM at 30 °C. The cellular concentration of aFib is unknown and therefore we cannot state with certainty that aFib mediated oligomerization is significant for sRNP function. However, abundant glycolytic enzymes have cellular concentrations approaching mM levels (Maughan *et al*., 2005) and it has been noted that aFib is an abundant cellular protein and eukaryotic Fib is the most abundant nucleolar protein (Eichler & Craig, 1994).

In addition to aFib*Sac*, three aFibs have been characterized in the literature. aFib self dimerization has now been observed in two archaeal species, *S. acidocaldarius* and *M. jannaschii*. aFib in complex with Nop5p (*A. fulgidus*) also forms a dimer but the

dimeric structure is mediated by Nop5p (Aittaleb *et al*., 2003; Aittaleb *et al*., 2004). aFib from *P. furiosus* has not yet been shown to form oligomers, however, it has only been characterized independently and may also form Nop5p mediated dimers.

Functional box C/D sRNP particles are comprised of two sets of proteins (aFib, Nop5p, L7Ae) assembled around the conserved box C/D and C'/D' sequences of a single guide sRNA. Work from two independent laboratories demonstrates this symmetric assembly is required for efficient methylation (Rashid *et al*., 2003; Tran *et al*., 2003). Studies performed on box C/D proteins from *A. fulgidus* show that aFib/Nop5p heterodimers self dimerize (Aittaleb *et al*., 2003; Aittaleb *et al*., 2004). Based on this work, it is currently accepted that the aFib/Nop5p multimeric complex forms the structural framework of the fully functional box C/D sRNP (Figure 6B). Association of the aFib/Nop5p complex at the strictly conserved terminal box C/D motif places a second catalytic unit approximately 80 Å away (Figure 6B). Conserved spacing of sRNA target regions and hybridization of guide and target RNAs limits the distance between residues methylated at the C/D and C'/D' motifs. It has been noted that the 80 Å inter active site distance resulting from Nop5p homodimerization exceeds the maximum distance possible between methylated residues (Tran *et al*., 2003). The ability of aFibs to form dimers, demonstrated above, suggests an alternate sRNP organization may exist whereby

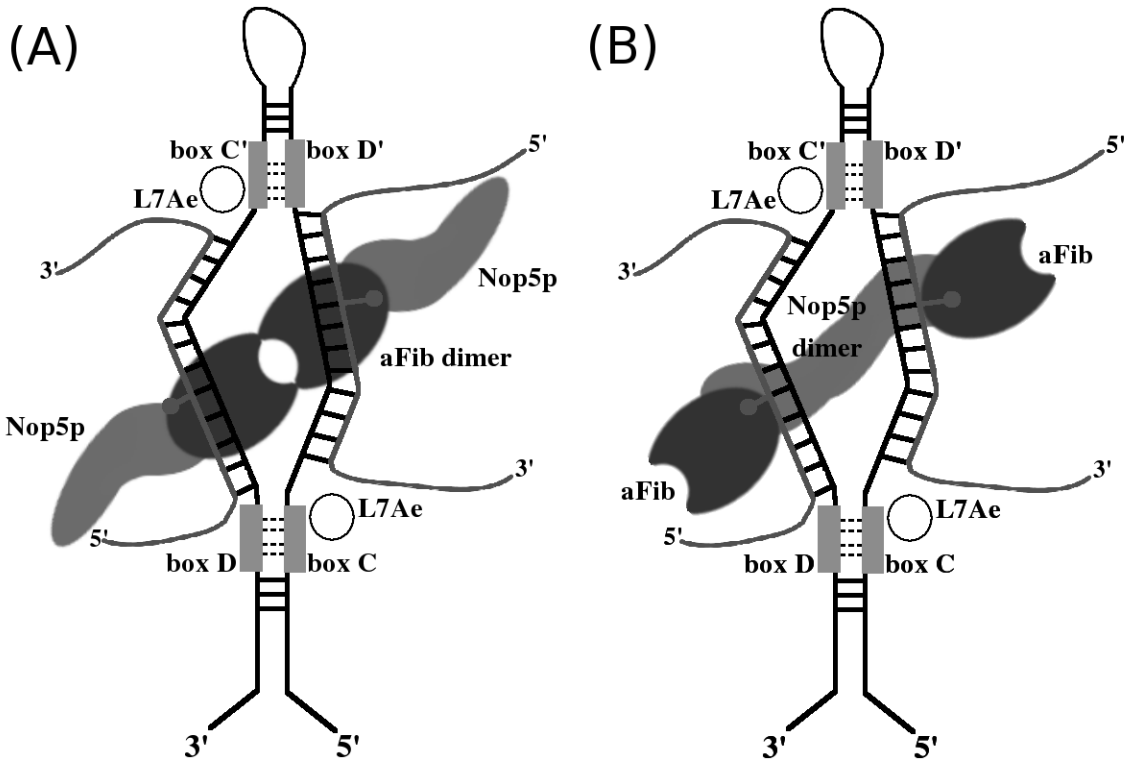

Figure 6: Box C/D sRNP complexes with (A) aFib amino terminal dimers or (B) Nop5p dimers as internal dimer between catalytic units. (Modified from Clouet-d'Orval et al., 2005).

an aFib dimer is the internal sRNP dimer (Figure 6A). This construct places the second catalytic site approximately 65 Å from the first. This distance is far more reasonable for correct positioning of aFib active sites at methylated residues, given system limitations. Although aFib dimerization is not conserved *in vitro* these studies do not preclude conservation of aFib dimerization in the presence of guide sRNAs.

At the supramolecular level, aFib dimerization may play a role in the stabilization of the pre-rRNA multi-box C/D sRNP complexes suggested by Fournier and Maxwell (1993). Sedimentation analysis of snoRNP complexes identifies two distinct groups; individual snoRNPs associated with pre-rRNA of approximately 10 S and larger, multi-

snoRNP complexes of 70-90 S, comprised of 2 or more snoRNP particles (Parker & Steitz, 1987; Reddy & Busch, 1988; Warner, 1990; Kiss *et al*., 1992; Sollner-Webb *et al*., 1996). These results suggest that eukaryotic snoRNPs may polymerize to form multi-snoRNP complexes while processing pre-rRNA. Polymerization of box C/D methylation complexes requires interaction at three protein-protein dimerization interfaces. In archaea, the formation of aFib/Nop5p heterodimers as well as aFib and Nop5p homodimers will result in the polymerization of box C/D sRNP particles in either assembly proposed in Figure 6. Due to the high similarity shared between core archaeal and eukaryotic pre-rRNA processing components the eukaryotic pre-RNA box C/D multi-snoRNP will likely have similar construction.

The demonstration that aFib*Sac* dimerizes adds to existing evidence that sRNPs function as dimers or even higher order oligomers. The measured dimerization constant is sufficiently low and the likely concentration of aFib*Sac* is sufficiently high that aFib*Sac* mediated dimerization of the sRNP may be functionally significant. Finally, aFib*Sac* mediated dimerization or polymerization of sRNP particles may explain supramolecular structures associated with RNA maturation or the ability of sRNPs to bind a wide variety of sRNAs and substrates.

In order to rationalize the inability of some aFibs to form dimers experimentally

and more completely understand the functional implications of aFib dimerization, including its potential effects in sRNP organization, it is important to understand the mechanism of this interaction. Wang *et al*. (2000) identified the amino terminal domain of aFib*Mja* as the putative dimerization domain of the crystallographic dimer. Although this is the most likely site for dimerization based on crystalline contacts, inspection of the aFib*Mja* structure identifies alternative, potential dimerization surfaces involving the carboxyl terminal domain. Therefore, in order to elucidate further the mechanism of aFib*Sac* dimerization, an amino terminal domain mutant was generated and subjected to biophysical assays similar to those applied to wildtype aFib*Sac*. The following chapter presents and discusses this work.

Chapter 3 - The aFib*Sac* dimerization domain

3.1 - Introduction

To date, partial characterization of aFib from three species have identified one homolog that self dimerizes. Wang *et al*. (2000) predicted that aFib*Mja* forms specific homodimers mediated by the amino terminal domain (Figure 7). Alternately, aFib from *A. fulgidus* forms heterodimers with Nop5p; the aFib/Nop5p interface involves a large hydrophobic patch on the surface of the carboxy terminal domain (Figure 7) (Aittaleb *et al*., 2003). In the absence of Nop5p, interaction at either interface could result in aFib*Sac* homodimers shown to form in chapter 2. In order to elucidate the mode of aFib*Sac* dimerization an amino terminal mutant was readily generated and biochemical tests, performed on wildtype aFib*Sac*, were repeated on this mutant.

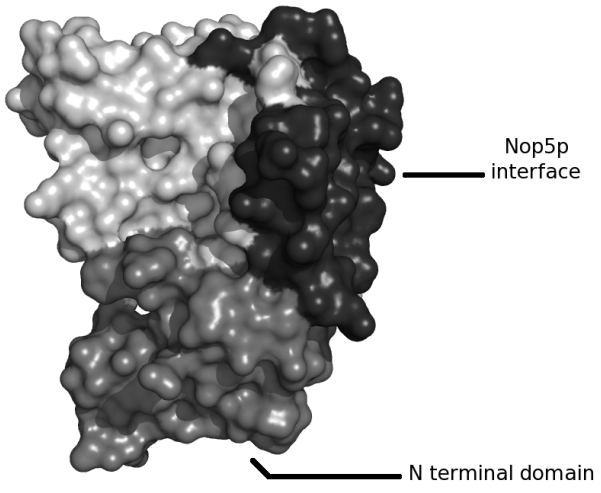

Figure 7. Molecular surface representation of structurally and functionally relevant regions of aFibSac. The amino terminal domain is shown in gray and the Nop5p interface in black. Figure generated in ***PyMOL*** *(DeLano Scientific, San Carlos, CA)*

Engineering an appropriate amino terminal aFib*Sac* mutant was based on an aFib*Sac* homology model constructed from the homologous, solved, three dimensional structure of aFib*Mja* (Wang *et al*., 2000). Homology modeling is highly accurate in predicting the common core of proteins and is an essential tool in the rational design of protein mutants (Schwede *et al*., 2000). The amino acid sequence identity between aFib*Sac* and aFib*Mja* is 51% and well above the threshold for safely assuming they share a common fold (Chothia & Lesk 1986).

The modeled aFib*Sac* structure consists of an amino-terminal β domain (residues 1-56) and a carboxy terminal α + β domain (residues 57-228). To test the hypothesis that aFib*Sac* dimerization is mediated by the amino terminus, an amino terminal mutant lacking the entire amino terminal domain was generated (Figure 8). Ideally, complete removal of the amino terminal domain minimizes the chance of partial or complete denaturation of the aFib*Sac* mutant. Data presented in this chapter indicates this mutant folds into a compact state and, therefore, experiments similar to those performed on wildtype aFib*Sac* were used to determine the ability of this mutant to form dimers.

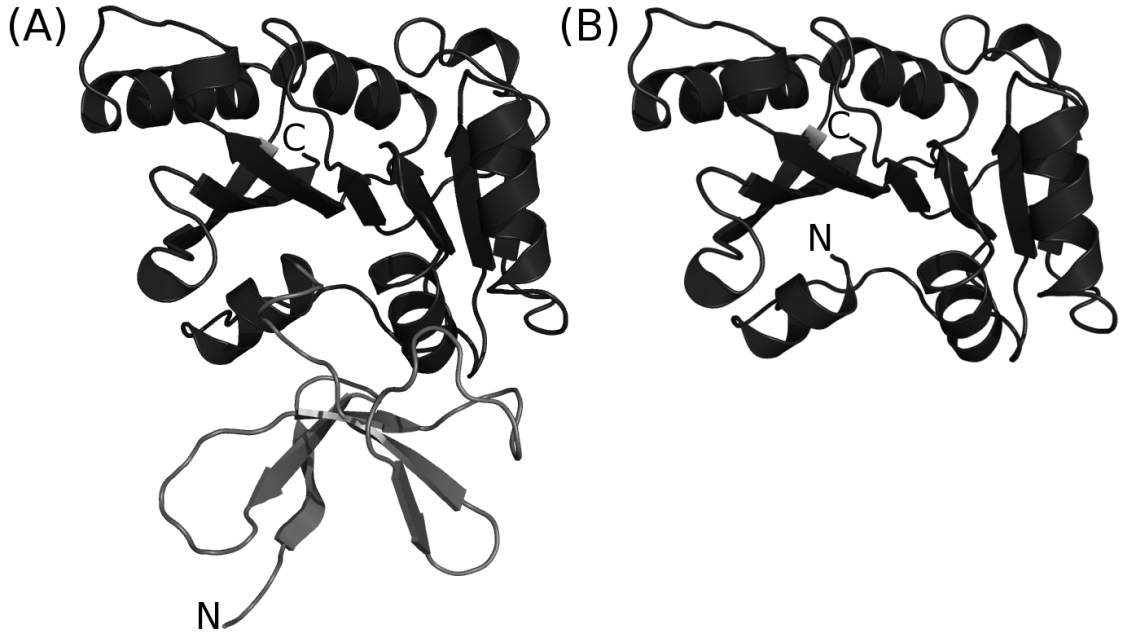

Figure 8. (A) Comparative model of aFib*Sac. The amino terminal domain is shown in light gray and the carboxy terminal domain in dark gray. (B) The aFibSac 56 residue amino terminal truncation mutant. Amino and carboxy termini of each model are indicated by the letters N and C respectively. Figure generated in* ***PyMOL (****DeLano Scientific, San Carlos, CA).*

3.2 – Methodology

3.2.1 - Cloning of recombinant aFib*Sac with amino terminal domain truncation:*

A mutant lacking the amino terminal domain was generated via modified inverse polymerase chain reaction (PCR) as outlined in Hemsley *et al.* (1989) and Rabhi *et al.* (2004). A pET28a cloning vector with the *S. acidocaldarius* fibrillarin gene sequence (GenBank Accession: AF201093) inserted at the *NheI* site of the cloning region served as the template DNA. Forward primer [5'- TTT AGA AGT AAG CTT GCG GGA -3'] complementary to the aFib*Sac* gene region 168 base pairs (56 residues) downstream of the start codon and reverse [5'- GCT AGT CAT ATG GCT GCA GC -3'] primer complementary to the 3' to 5' end of the pET28a vector at the *NheI* cut site were used to generate a 6x His tagged aFib*Sac* mutant with 56 amino acids truncated at the amino terminus; all primers were phosphorylated at the 5' end. The PCR reaction mixture was comprised of 1X *P. furiosus* (PFU) DNA polymerase reaction buffer with 2 mM $MgSO_4$ (Fermentas International Inc., Ontario, Canada), 2 mM of each deoxynucleoside triphosphate, 0.5 μM of each forward and reverse primer, 15 nM of template DNA, and 1.25 Units PFU polymerase. Amplification was performed for 30 cycles of 94 °C (15 seconds), 54 °C (30 seconds) and 70 °C (14 minutes).

3.2.2 - Expression and purification of recombinant aFib*Sac with amino terminal domain truncation:*

Over expression and purification of the 6x His tagged aFib*Sac* mutant lacking amino acids 1-56 (aFib*Sac*_N23n56) was performed as described in section 2.2.1 for aFib*Sac*_N23. The amino terminal 6x His tag of aFib*Sac*_N23n56 was removed at the thrombin cleavage site, resulting in aFib*Sac*_N6n56. Cleaved protein was separated by a Ni-NTA as described previously (section 2.2.1) and injected onto an SEC equilibrated in buffer B. Elution profiles of aFib*Sac*_N6n56 exhibit a single peak at the expected molecular weight of the monomer. This indicates the aFib*Sac*_N6n56 mutant protein folds into a compact state and is not denatured.

3.2.3 - Size exclusion chromatography of aFib*Sac_N6n56:*

An aFib*Sac*_N6n56 sample (300 mL) at 249.2 μM was injected onto a SEC column and run as described in section 2.2.3. Apparent molecular weights were estimated by comparing the elution volume of aFib*Sac*_N6n56 to a standard curve constructed using size exclusion protein standards.

3.2.4 - Isothermal titration calorimetry of aFib*Sac_N6n56:*

ITC experiments were performed and data analyzed as described in section 2.2.5.

3.3 – Results

3.3.1 - Size exclusion chromatography analysis of aFib*Sac*_N6n56*:*

SEC experiments, under native conditions, were performed on the amino terminal mutant aFib*Sac*_N6n56 to determine the quaternary structure of aFib*Sac* in the absence of its amino terminal domain. A representative chromatogram for aFib*Sac*_N6n56 is presented in Figure 9. At a concentrations of 249.2 μM aFib*Sac*_N6n56 elutes as a single peaks at 16.65 mL, corresponding to a molecular weight of 22.4 kDa. This compares well with the monomer molecular weight calculated from the sequence (20.5 kDa) and suggests the enzyme is a monomer at these concentrations. This concentration is well above both the K^d (60.9 μM) determined by ITC for wildtype aFib*Sac* and the concentrations of wildtype aFib*Sac* that give rise to both monomers and dimers by SEC. This mutant shows no evidence of forming oligomers at 249.2 μM and suggests the amino terminal domain is directly involved in dimerization.

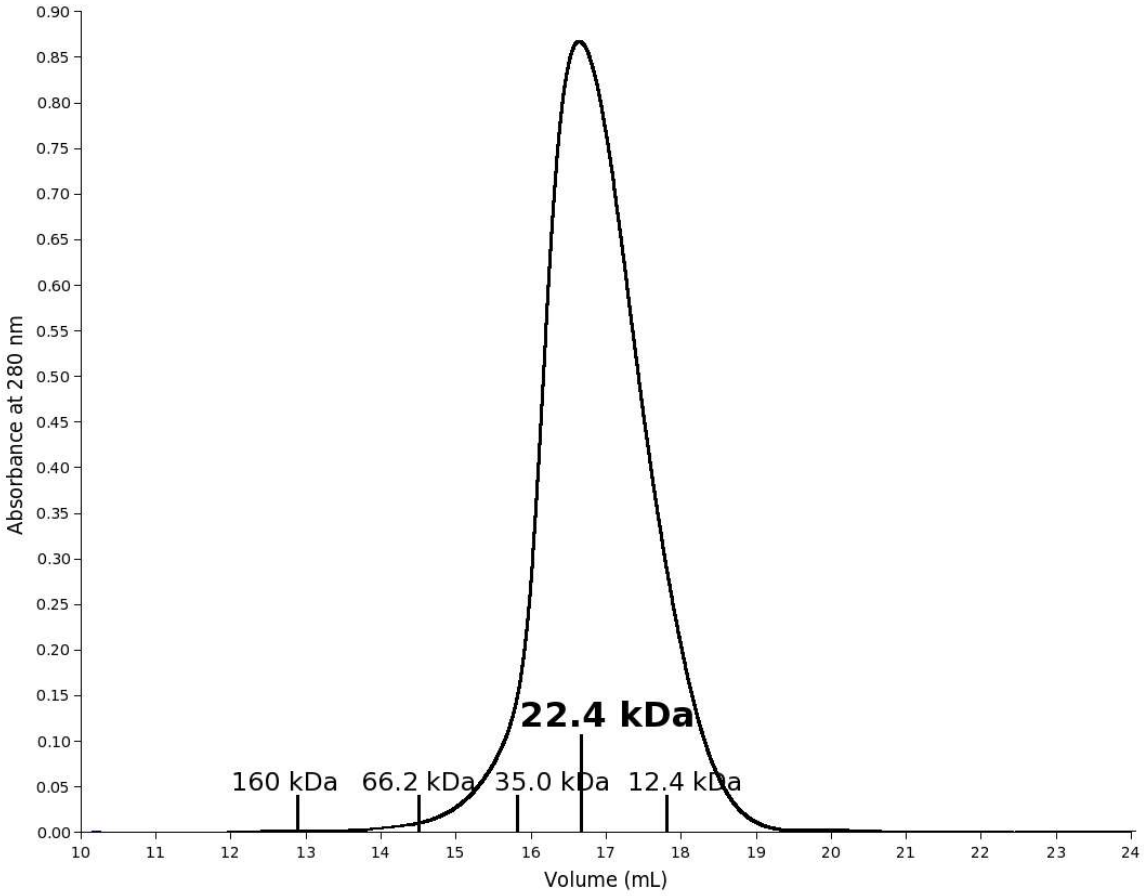

Figure 9: Size exclusion chromatography of aFib*Sac_N6n56 showing the UV absorbance at 280 nm as a function of elution volume. 400 µL of* aFib*Sac_N6n56 at 249.2 µM was run on a SuperdexTM 200 column. Elution volumes of protein standards are marked along the volume axis and corresponding molecular weights noted above. Absorbance at 280 nm is a logarithmic measure of optical density.*

3.3.2 - Isothermal titration calorimetry experiments on aFibSac_N6n56:

ITC experiments were performed on aFib*Sac*_N6n56 through the concentration range 256 to 6.37 µM. A representative titration curve is presented in Figure 10. Enthalpy measurements for the aFib*Sac*_N6n56 system over this concentration range indicate no change in enthalpy above that observed for a titration of a buffer system.

A clear, sigmoidal transition was observed in the enthalpy change for purified, wildtype aFib*Sac* as it was titrated through the concentration range 63.6 and 60.3 μM. Based on data provided by SEC and sedimentation velocity experiments this transition was interpreted as an indication of the dimer to monomer transition. By comparison, the constant, small ΔH observed in ITC experiments on aFib*Sac*_N6n56 suggests that, unlike the wildtype system, no large change in the protein conformation or quaternary structure occurs through the concentration range tested.

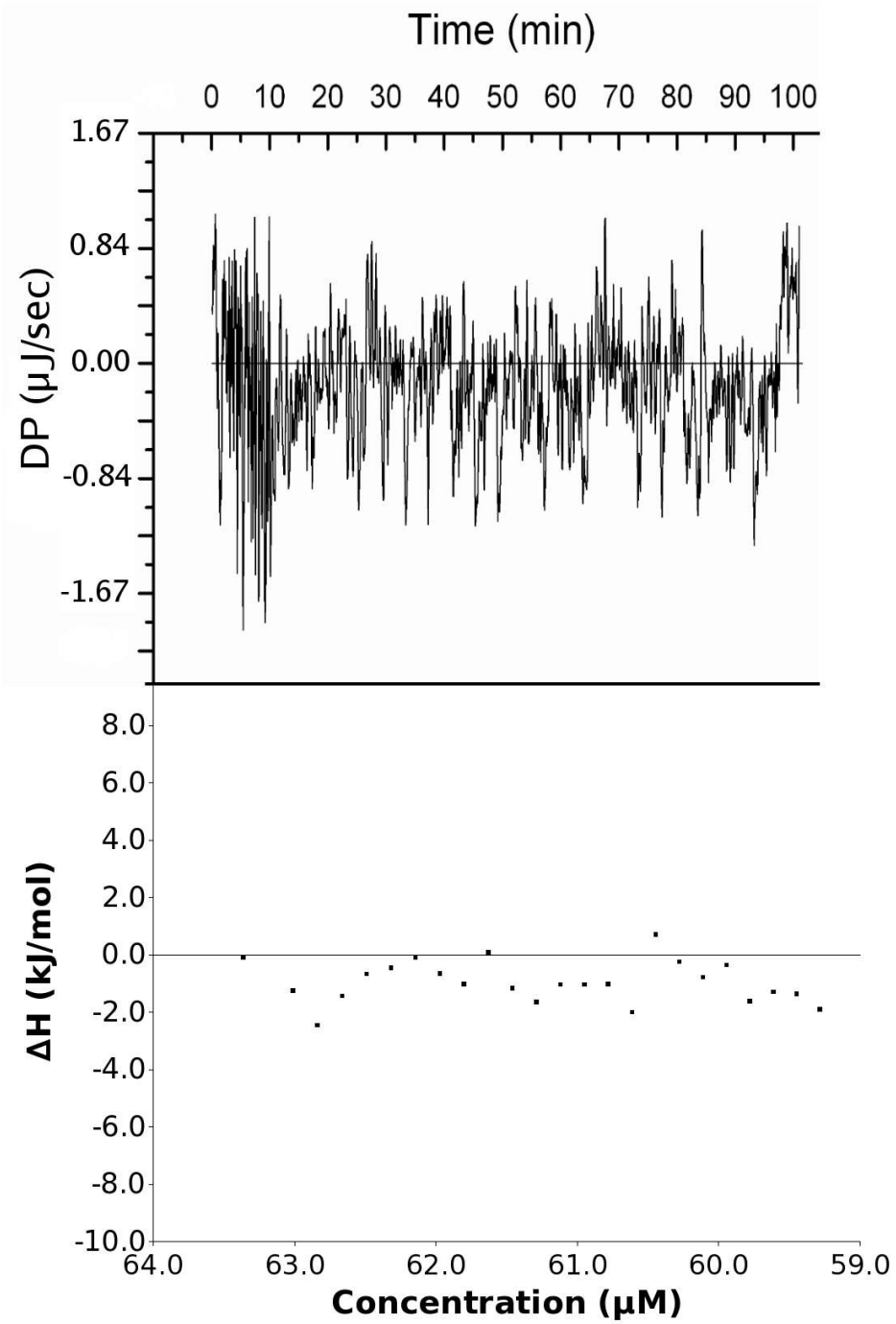

Figure 10: Differential power as a function of time data obtained for injections of buffer into aFib*Sac_N6n56 protein solution at 62.39 µM (upper panel). The enthalpy of association of* aFib*Sac_N6n56 as a function of concentration as determined by ITC at 30 °C, no transition detected.*

3.4 – Discussion

Here we provide evidence the amino terminal domain of aFib*Sac* is an essential component of concentration-dependent dimerization. Two potential protein-protein interaction sites have been identified for aFibs; first, a portion of the amino terminal domain that forms a crystallographic dimer, as observed by Wang (2000) and second, a carboxy terminal region which is the site of Nop5p binding (Aittaleb *et al*., 2003). A mutant lacking the amino terminal domain was readily constructed, over expressed and assayed for dimer formation.

The amino terminal domain mutant is soluble and appears to fold into a native-like state. A single elution peak at the expected monomer molecular weight from SEC experiments and the formation of aFib*Sac*_N6n56 crystals (Figure 11), with discernible diffraction patterns, indicate that the aFib*Sac*_N6n56 mutant is able to fold into a compact conformation (Bernal & Crowfoot, 1934) and, therefore, biophysical assays similar to those applied to wildtype aFib*Sac* were performed.

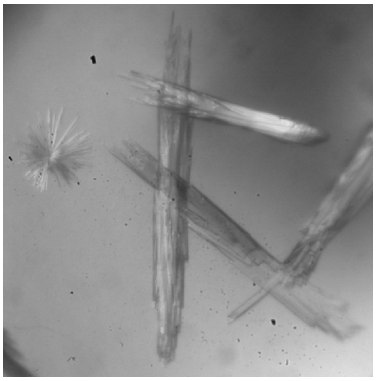

Figure 11: aFibSac_N6n56 crystals. Crystals were grown at 37 °C by vapor diffusion in 100 mM MES (pH 6.5), 12% polyethylene glycol 6000 and 0.1% Triton mixed 1:1 with 350 μM aFibSac_N6n56.

SEC experiments performed on aFib*Sac*_N6n56 demonstrate that, under conditions where dimers of wildtype aFib*Sac* are observed, the amino terminal deletion abolishes dimerization. Work presented in chapter 2 demonstrates that aFib*Sac* can form dimers in a concentration dependent manner with a 61.9 μM dissociation constant. Titration experiments of aFib*Sac*_N6n56 suggest that, unlike the wildtype system, no large conformational change occurs as a function of concentration. These results provide evidence that the amino terminal domain is responsible for dimerization of aFibs.

Currently, of the aFibs with solved three dimensional structures, only aFib*Mja*, and now aFib*Sac*, have been show to homodimerize. Despite being structurally homologous, aFib*Afu* and aFib*Pfu* are monomeric *in vitro* (Aittaleb *et al*., 2003; Deng *et al*., 2004). This discrepancy is examined further in Chapter 4 and a model that rationalizes reports that aFibs from different species have different quaternary structures is proposed and tested.

Chapter 4 - The site of aFib*Sac* dimerization

4.1 - Introduction

The four aFibs characterized to date share between 35 and 52% amino acid sequence identity in pairwise comparisons. This significant sequence identity gives rise to closely similar structures as indicated by root mean square deviations of 0.06 to 0.99 Å in C^a atomic coordinates of the superposed structures. In chapters 2 and 3, aFibSac was shown to form dimers mediated by the amino terminal domain at near physiological conditions similar to reports for aFib*Mja* (Wang *et al*., 2000). Alternately, aFib*Afu* and aFib*Pfu* are exclusively monomeric (Aittaleb *et al*., 2003; Deng *et al*., 2004). Given the levels of sequence and structural similarity between aFibs, what structural determinants account for differences in aFib oligomeric state? While there are many potential interactions that may contribute to the formation of dimers, we note that the amino terminal domain of the aFibs have a significantly lower sequence identity, greater sequence length variation and, thus, higher rmsd in comparison with the catalytic carboxy terminal domain.

We note that the amino terminal domains of aFib*Sac* and aFib*Mja* are larger than those in the aFibAfu and aFibPfu. The dimerization interface observed in the aFib*Mja*

structure primarily involves main-chain hydrogen bonding interactions between the amino terminal β1' and the β4' strands of independent subunits, forming an elongated 10 stranded β-barrel (Figure 12; Wang *et al*., 2000). Due to the two-fold symmetry of the dimerization interface, a decrease in the length of the amino termini reduces the number of atoms available for inter-subunit interactions, thereby destabilizing the interface at two independent sites (Figure 12).

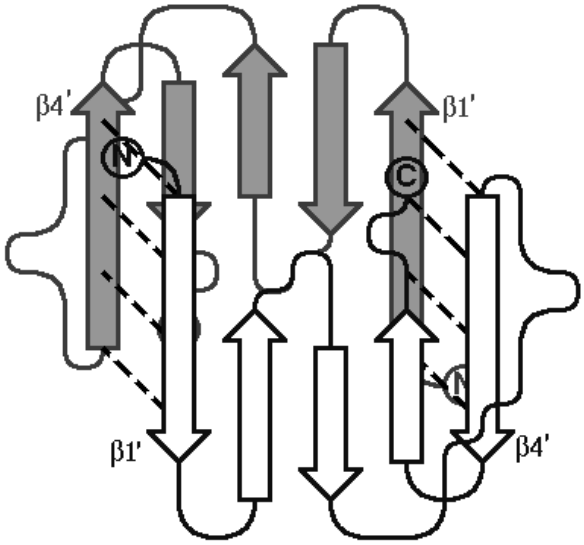

Figure 12: 2D topology representation of the β-barrel formed from the association of the amino terminal domains of independent aFib subunits. Secondary structures involved are marked and named according to Wang et al. (2000). N indicates the amino termini of each subunit and C represents where the structure continues on to the carboxy terminal domain.

Evolution has resulted in several mutations within the secondary structures of the β-barrel at the aFib amino terminal dimerization interface. Truncation of the extreme amino terminus was the mutation most readily replicated experimentally. Therefore, an aFib*Sac* mutant with an eleven residue amino terminal truncation was generated (Figure

13). This mutant will have an amino terminus identical in length to aFib*Pfu* which is monomeric in solution. Initial experiments assessing the ability of this mutant to form oligomers were then performed.

Figure 13: Homology model of aFib*Sac. Amino and carboxy termini are marked with N and C respectively. The residues truncated in the amino terminal mutant are shown in white. Figure generated in* ***PyMOL*** *(DeLano Scientific, San Carlos, CA).*

4.2 – Methodology

4.2.1 – Molecular superposition and structural alignments of solved aFibs*:*

Swiss PDB viewer (**SPDBV**; Guex & Peitsch, 1997) was used to perform molecular superposition and root mean square deviation calculations between the aFib*Sac* comparative model (section 2.2.2) and solved three dimensional structures of fibrillarin homologs from *M. jannaschii* (Wang *et al*., 2000), *A. fulgidus* (PDB accession: 1NT2 chain A; Aittaleb *et al.*, 2003) and *P. furiosus* (PDB accession: 1PRY; Deng *et al.*, 2004). The resulting superpositions were used to generate the structure-based sequence alignment.

Accessible and buried surface areas for individual residues and secondary structures within each model were computed using **CCP4** (1994). Total buried surface area was calculated as the difference in accessible surface area between twice the monomer and corresponding dimer.

4.2.2 – Cloning, over-expression and purification of recombinant aFib*Sac with truncation of the amino-terminal β-strand:*

A mutant lacking 11 amino acids at the amino terminus was generated via modified inverse PCR from the wild pET28a gene construct (see section 3.2.1). Forward primer [5'- TTC GAC AAC GTA TAT GAA TGC AT -3'] complementary to the

aFib*Sac* gene region downstream of the start codon corresponding to amino acid sequence starting at residue 12 and reverse primer [5'- GCT AGT CAT ATG GCT GCA GC -3'] complementary to the 3' to 5' end of the pET28a vector at the *NheI* cut site, were used to generate a 6x His tagged aFib*Sac* mutant with 11 amino acids truncated at the amino terminus. PCR mixtures and conditions are outlined in section 3.2.1.

Over expression and purification of the 6x His tagged aFib*Sac* mutant lacking amino acids 1-11 (aFib*Sac*_N23n11) were performed as described in section 2.2.1 for aFib*Sac*_N23. The amino terminal 6x His tag of aFib*Sac*_N23n11 was removed at the thrombin cleavage site, resulting in aFib*Sac*_N6n11. Cleaved protein was separated by a Ni-NTA column as described previously (see section 2.2.1) and injected onto a SEC column equilibrated in buffer B. The elution profile of aFib*Sac*_N6n11 exhibited a peak at the expected molecular weight, suggesting this recombinant mutant protein folds into a compact state.

4.2.3 - Size exclusion chromatography of aFib*Sac_N6n11:*

An aFib*Sac*_N6n11 sample (300 mL) at 170.2 μM was injected onto a S200 SEC column and run as described in section 2.2.3. Apparent molecular weight was estimated by comparing the elution volume of aFibSac_N6n11 to a standard curve.

4.3 – Results

4.3.1 – Structural comparison of solved aFibs *amino termini:*

The root mean square deviation (rmsd) calculations performed pair-wise between the carboxy terminal catalytic domains of solved aFib homologs and the aFib*Sac* model indicate a high degree of structural similarity based upon rmsd values around or below 1.0 Å (Table 2). Conversely, rmsd calculations performed on the amino terminal domains of these structures show significantly less structural conservation than the catalytic domain (Table 3).

Table 2: Root mean square deviation values of pair-wise comparison with no restraints of aFib*Sac*, aFib*Afu*, aFib*Pfu, and* aFib*Mja carboxy terminal domain Cα atoms. The number of residues used for each calculation are indicated below the RMS value.*

	aFib*Sac*	aFib*Afu*	aFib*Pfu*
aFib*Mja*	0.15 Å 155	0.93 Å 145	0.78 Å 156
aFib*Pfu*	0.80 Å 151	1.01 Å 144	
aFib*Afu*	0.94 Å 143		

Table 3: Root mean square deviation values of pair-wise comparison with no restraints of aFib*Sac,* aFib*Afu,* aFib*Pfu, and* aFib*Mja amino terminal domain Cα atoms. The number of residues used for each calculation are indicated below the RMS value.*

	aFib*Sac*	aFib*Afu*	aFib*Pfu*
aFib*Mja*	0.09 Å	1.40 Å	1.08 Å
	50	36	47
aFib*Pfu*	1.07 Å	1.42 Å	
	47	35	
aFib*Afu*	1.49 Å		
	39		

Molecular superposition and the resulting structural alignment of amino terminal domains highlights the differences in length of aFib amino terminal β strands (Figure 14). The dimerization interface of the modeled aFib*Sac* dimer has a buried surface area of approximately 1300 $Å^2$ and involves eight inter-subunit main-chain to main-chain hydrogen bonds.

Structural alignment of solved aFib amino terminal domains shows that several deletion mutations occur within the amino terminal domain of aFib*Afu* (Figure 14). As a result, the amino terminal domain of aFib*Afu* is considerably smaller than that of the remaining three aFibs, this may result in the inability of aFib*Afu* to form homodimers. However, the amino terminal domain of monomeric aFib*Pfu* is comparable in size to dimeric aFibs. Inspection of the barrel formed by amino terminal dimerization places

certain residues within the hydrophobic core of the barrel. In the aFib*Sac* modeled dimer, residues indicated in Figure 14 (black dots below the sequence) are within the core. Interestingly, residues that align to Phe20 in aFib*Sac* are not conserved between monomeric and dimeric aFibs (Figure 14, boxed). The introduction of a charged residue, Asp17 and Asp12 in aFib*Pfu* and aFib*Afu* respectively, within the hydrophobic core of the barrel may result in its destabilization. However, Phe20 is partially solvent accessible, therefore, rotation around the χ^1 torsion angle would remove the charge of the substituted Asp from the β-barrel core.

In silico step-wise truncations of residues at the amino terminus of the modeled aFib*Sac* structure indicates that removal of two amino acids reduces the buried surface area of the respective dimer below the theoretical threshold for a dimer. As seen in Figure 14, deletion of the first two amino terminal residues resolved in the modeled aFib*Sac* structure (aFib*Sac*_N6n11 mutant, Figure 14) results in a strand identical in length to the amino terminal strand resolved in the aFib*Pfu* structure, which is exclusively monomeric in solution.

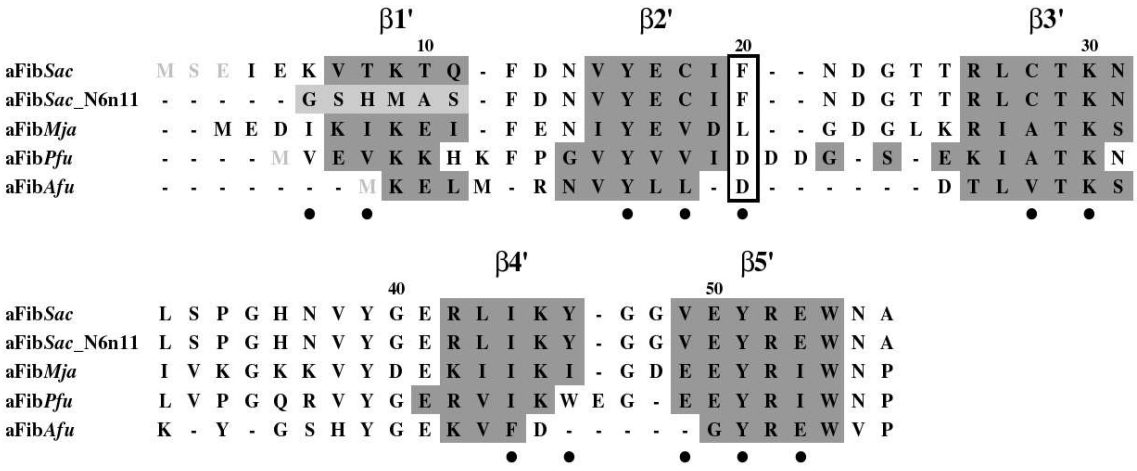

Figure 14: Structural alignment of aFib amino terminal domains. Residues not resolved in modeled structures are in light gray text. Secondary structures are highlighted by gray blocks and are labeled above as outlined by Wang et al. (2000). Residues within the hydrophobic core of the β-barrel are indicated by circles below the sequence. Residues with greatest deviation in physiochemical properties between aFibs are outlined by a black box. Sequence number of aFibSac is indicated above the sequence. Residues from 6x His tag remaining after thrombin cleavage are highlighted by light gray block.

4.3.2 - Size exclusion chromatography analysis of aFib*Sac*_N6n11*:*

At a concentration of 170.2 μM aFib*Sac*_N6n11 elutes as a single peak at 16.33 mL (Figure 15, solid trace). Compared to the elution profiles observed for aFib*Sac* (Figure 15, dashed trace), this mutant behaves similarly to aFibSac_N6n56 and shows no evidence of forming oligomers. aFib*Sac*_N6n11 has a smaller apparent molecular weight of 26.4 kDa.

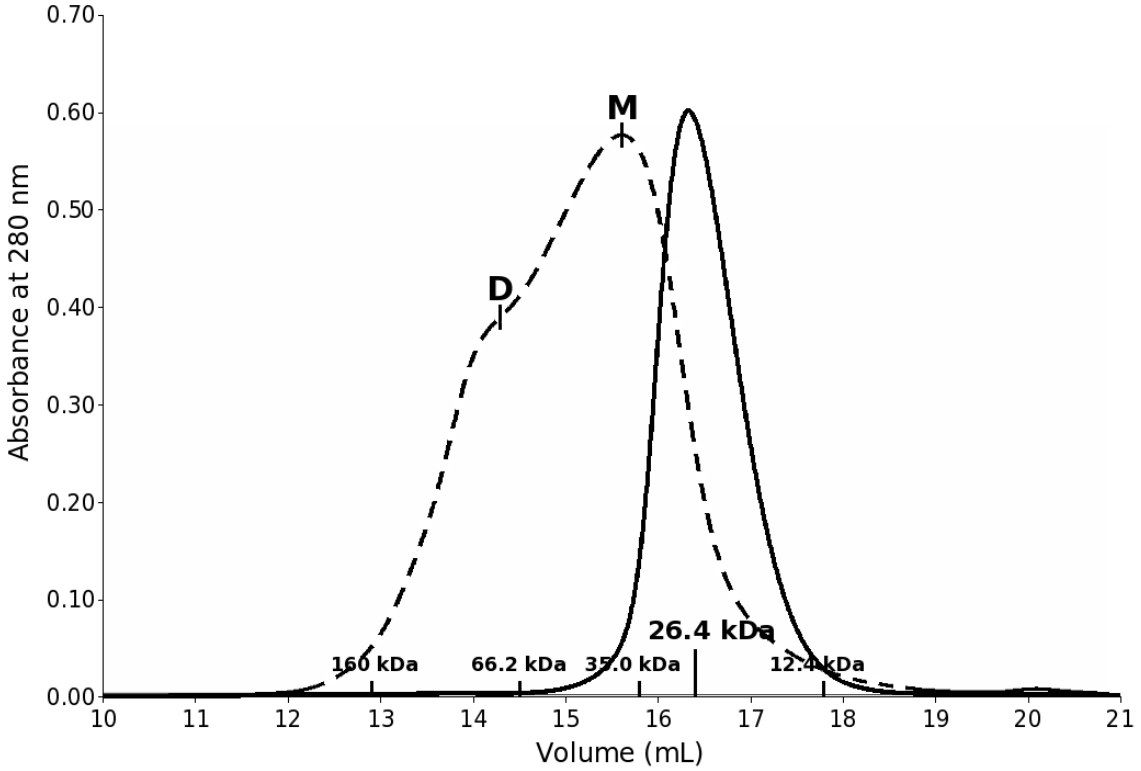

Figure 15: Size exclusion chromatography of aFibSac_N6n11 (solid trace) showing the UV absorbance at 280 nm as a function of elution volume. 400 μL of aFibSac_N6n11 at 170.2 μM was run on a SuperdexTM 200 column. Elution volumes of aFibSac_N6n11 sample and protein standards are marked along the volume axis and corresponding molecular weights noted above. Wildtype aFibSac SEC elution profile is shown as a dashed line, dimer and monomer peaks are indicated by "D" and "M" respectively.

4.4 – Discussion

Here we provide evidence that the amino terminal β1' strand of aFib*Sac* is essential for dimerization. Modeling studies indicate removal of the amino terminal β1' strand disrupts main-chain to main-chain hydrogen bonds between subunits, reduces the buried surface area of the modeled dimer below the accepted threshold for a dimer and abolishes dimerization. A mutant with amino terminus just below the predicted buried surface area threshold required for a dimer is monomeric in solution (Chothia and Janin, 1975), as demonstrated by SEC. As seen in Figure 14, this amino terminal strand is significantly shorter (*P. furiosus*) or absent (*A. fulgidus*) in aFibs that are monomeric. *M. jannaschii* aFib has additional amino terminal residues relative to monomeric aFibs that contribute to a longer β1' strand and forms a dimer. The aFib*Sac* amino terminus is longer than *M. jannaschii* aFib (Figure 14B) and also forms dimers as demonstrated in chapter 2. Since the dimerization interface involves interaction between two amino terminal β1' strands and two β4' strands, one from each aFib subunit, differences in the β1' strand length strongly affect the buried surface area.

Based on these data, we propose that aFib dimerization depends on the buried surface area of the dimer which in turn is largely dependent upon the length of the β1' strand. This simple model successfully rationalizes reports that aFibs from different

species are dimers (Wang *et al*., 2000) or exclusively monomers (Aittaleb *et al*., 2003; Deng *et al*., 2004). Our model predicts aFibs with an amino terminal β1' strand as long, or longer than that of aFib*Mja* will form dimers independent of interactions with additional sRNP components.

Several arguments have been put forward suggesting aFibs are likely monomeric. Firstly, Aittaleb *et al*. (2003) cite the association of aFib/Nop5p heterodimers as evidence supporting the view that aFibs are exclusively monomers. While the observed heterodimer supports the formation of Nop5p mediated dimers it does not exclude the formation of aFib dimers. As seen in Figure 16 the aFib dimer proposed above does not disrupt the aFib/Nop5p heterodimer nor will it disrupt the self association of these heterodimers through the coiled-coiled domain of Nop5p (Figure 16, light purple domains). Second, lack of sequence conservation in the amino terminal domain suggests that amino terminal mediated aFib dimerization is improbable (Deng *et al*., 2004). This argument is valid for associations that depend upon side-chain mediated interactions. In this system, almost 70% of the observed and modeled interactions at the dimer interface are main-chain van der Waal and hydrogen bonding interactions that are independent of sequence. Thus the sequence similarity in this region is unimportant, provided a β-sheet can form and sufficient contacts are available to form the β-barrel.

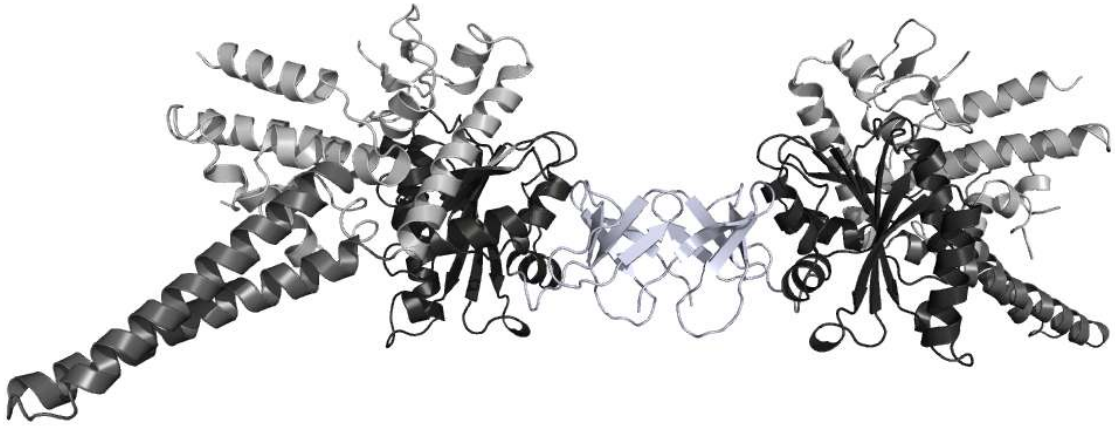

Figure 16: A model of a dimeric, archaeal aFib/Nop5p complex based upon the homology model of aFib from S. acidocaldarius and the known structure of A. fulgidus aFib/Nop5p. The N-terminal domain (white) of aFib facilitates dimerization and does not interfere with the association of Nop5p (light gray) and the C-terminal domain (black) of aFib nor does the proposed aFib dimer interfere with the self-association of Nop5p via coiled-coiled domains (dark gray). Figure generated in ***PyMOL*** *(DeLano Scientific, San Carlos, CA).*

In light of differences observed in the length of the amino termini of aFibs, demonstration that aFib*Sac* dimerization depends upon the the length of the amino terminus rationalizes reports that aFibs have been observed as monomers and dimers *in vitro*. This simple model will allow us to predict the potential of aFibs to form multimers and likely extends to eukaryotic counterparts.

Chapter 5 - Implications of aFib dimerization

5.1 – Dimerization of aFib in different archaeal species

In this work we demonstrate that aFibs can form homodimers mediated by the amino terminal domain similar to aFib dimers observed by Wang and coworkers (2000). This is consistent with the current model of two copies of protein subunits per guide sRNA. Additionally, we provide a model to rationalize the inability of aFibs with shorter amino terminal sequences from *A. fulgidus* and *P. furiosus* to form homodimers. This simple model allows us to predict if an aFib will homodimerize, based on primary sequence. Alignment of a representative sample of aFib sequences from the NCBI protein database was performed in **CLUSTALW** (Thompson et al., 1994) and is presented in Figure 17. This sequence alignment indicates the amino terminal domains of aFibs from seven archaeal species will likely not form the elongated 10 stranded β-barrel required for dimerization (Figure 17, red text). Based on our model, the remaining eighteen aFibs aligned have amino termini long enough that dimerization may occur provided a sufficiently long β1' strand can form.

5.2 – Inter and intra-sRNP interactions: The role of aFib and Nop5p

In addition to aFib amino terminal dimerization presented above, the aFib/Nop5p heterodimer self-dimerizes via the coiled-coiled domain of Nop5p (Aittaleb *et al*., 2003). We suggest that both dimerization mechanisms, could be utilized during the varied box C/D sRNP functions or during assembly. In either proposed sRNP complex homodimerization of aFib or the aFib/Nop5p heterodimer would result in the formation of functional C/D sRNP particles with two catalytic units. However, spatial limitations between methylated residues suggests the aFib dimer is the internal intra-sRNP dimer. The apparent conservation of the coiled-coiled domain of archaeal Nop5p proteins (data not shown) suggests this interaction is also functionally important. In our aFib dimer sRNP model, interaction of Nop5p at the coiled coiled domain will result in the formation of multi-sRNP complexes observed by Fournier and Maxwell (1993).

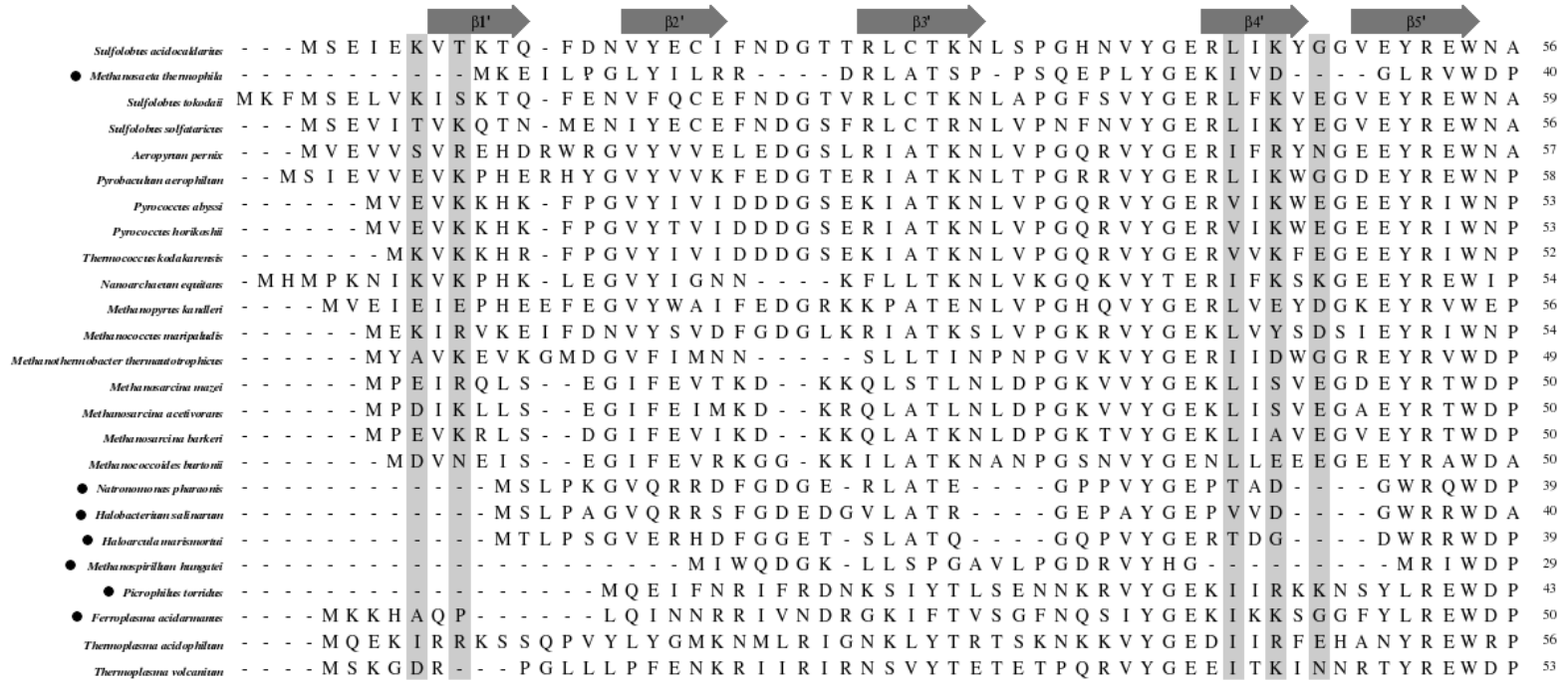

Figure 17: Sequence alignment of aFib amino terminal domains. Secondary structures of aFib from S. acidocaldarius are illustrated above sequences. aFibs which will not form amino terminal mediated dimers are shown in red text. Residues involved in inter-subunit hydrogen bonding are indicated in gray.

5.3 – Fib dimerization in Eukaryotes

Alignment of aFib and eukaryotic Fibs show that the amino terminal aFib domain aligns well within the eukaryotic amino terminal domain downstream of the GAR domain (Figure 18). The eukaryotic GAR domain is essential for localization of Fib to the nucleoli (Ghisolfi *et al*., 1992) and has been shown to aid in destabilizing RNA secondary structures (Heine *et al*., 1993). Fibs in some lower eukaryotes lack GAR domains (David *et al*., 1997; Russell *et al*., 2005) indicating that either the interaction with RNA may not be its key role or an alternative mechanism of aiding the destabilization of RNA secondary structure has evolved in these organisms (Amiri, 1994). Either way the main role of the eukaryotic GAR domain, nucleolar targeting, is sufficient for evolutionary inclusion in higher eukaryotes. Consequently, differences in eukaryotic Fib and aFib sequences arise from the evolution of cellular compartmentalization in eukaryotes.

While it is possible that Fib dimerization is conserved only in eukaryotes without GAR domains, as seen in Figure 18 the eukaryotic sequences are all expected to retain their overall fold and the potential to form amino terminal dimers. Experiments performed by Ghisolfi and coworkers (1992) show that the GAR domain forms a β-spiral *in vitro* and van Raaij *et al*. (1999) confirmed the residues adopt non-random conformations that result in an asymmetric supra-secondary structure. Based upon the

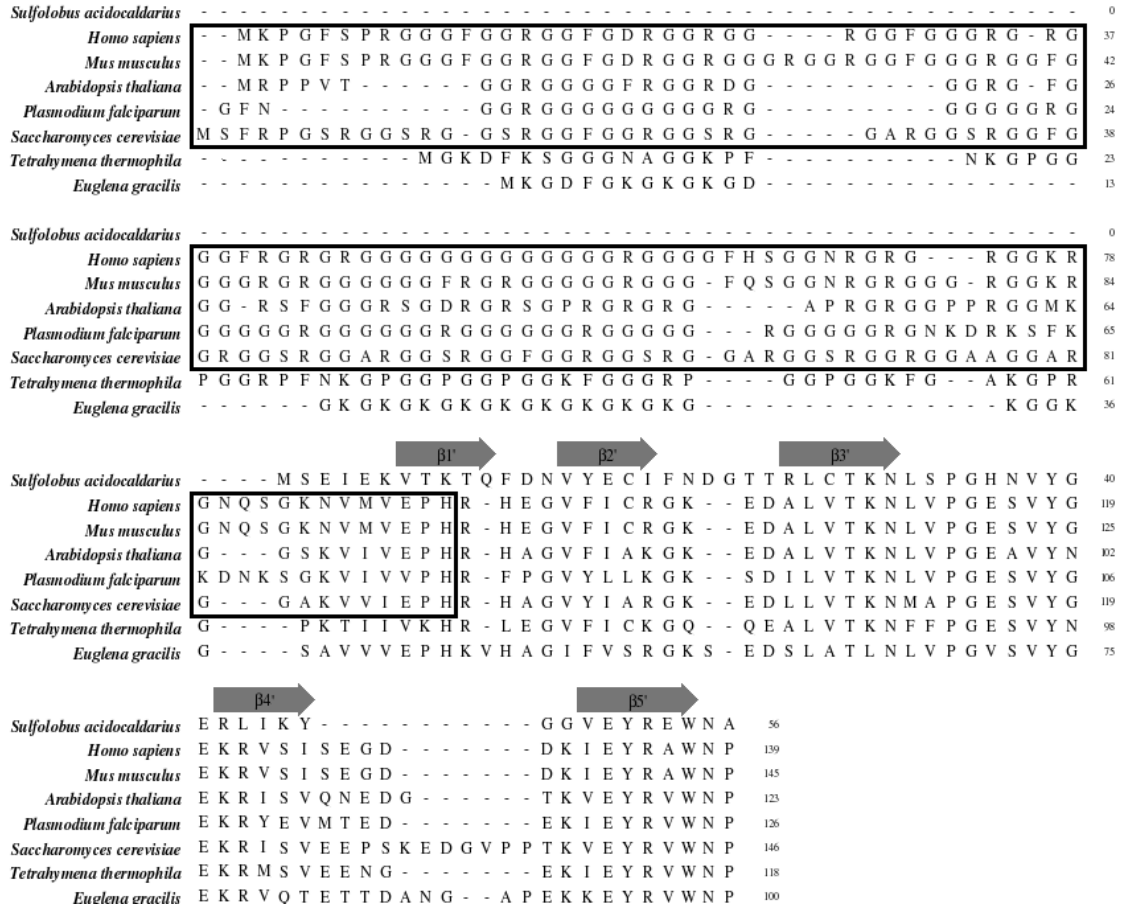

Figure 18: Sequence alignment of Fib from S. acidocaldarius and eukaryotic Fibs. Secondary structures of the aFibSac amino terminal domain are illustrated above sequences. Residues of the eukaryotic GAR domain are boxed.

known structures and our model the GAR domain is likely to extend away from the dimer interface leaving the eukaryotic amino terminal domain accessible for dimerization. Further, the expected domain structure allows for the accommodation of the GAR domain in both the amino terminal mediated aFib dimer and the aFib/Nop5p complex observed by Aittaleb *et al*. (2003). The evidence suggests that Fib dimerization may occur in both lower and higher order eukaryotes.

5.4 – Box C/D sRNP conformation and multi-tasking

Diversity in guide and substrate RNA requires molecular flexibility in the organization of sRNP (or snoRNP) components such as archaeal and eukaryotic fibrillarin. The quaternary structure(s) of sRNPs will have a role in the ability of these complexes to methylate various substrates. Box C/D sRNPs are known to methylate precursor rRNA of both eukaryotes and archaea. Recent works have identified additional roles of box C/D sRNP in the post-transcriptional methylation of various archaeal RNAs and eukaryotic cellular RNA. In vertebrates, classic or modified box C/D snoRNAs mediate the addition of 2'-O-methyl groups to U6 (Tycowski *et al*., 1998) and U5 (Kiss, 2001) spliceosomal RNA. Additionally, tissue specific snoRNPs have been shown to interact with mRNA and the resulting methylation of these molecules has been implicated in the regulation of messenger RNA (mRNA) editing (Ganot *et al*., 1999; Filipowicz, 2000). The homologous system in archaea methylates precursor tRNA (Gaspin *et al*., 2000; Omer *et al*., 2000; Clouet d'Orval *et al*., 2001, Ziesche *et al*., 2004) and is suggested to methylate archaeal mRNA (Armbruster & Daniels, 1997). In addition to the many substrates, the methylation complex must interact with numerous guide RNAs. Due to the abundance of aFib in the cell and its ability to methylate varied sequences, catalysis of target RNA methylation is regulated by the formation of box C/D sRNPs.

Efficient methylation requires two catalytic units per guide sRNA (Rashid *et al*., 2003; Tran *et al*., 2003) and, likely, interaction between independent box C/D sRNP particles (Fournier & Maxwell, 1993). The role of aFib dimerization is not yet known, it is reasonable to suggest that aFib dimers may aid or even be required for catalysis in some species and will be the focus of future studies.

The box C/D methylation complex is one of many essential sRNP particles in the cell that may adopt multiple conformations. The ribosome is another highly dynamic RNP having several well-defined conformations during the peptide elongation cycle. Similarly the RNP particles telomerase and spliceosomes undergo protein reassembly during catalysis. This work on the catalytic component of the box C/D sRNP methylation complex adds to the current repertoire of RNP complexes that have been studied and suggest it will be another highly dynamic structure.

5.5 – Future studies

As outlined in this brief summary, we have rationalized contradictory evidence regarding aFib quaternary structure. This work adds to our current understanding of aFib *in vitro* and, potentially, its assembly into the box C/D sRNP complex. Continuing efforts to understand the structure and function of box C/D sRNP particles work will

focus upon protein-protein and protein-RNA interactions required for assembly, binding and catalysis and how these interactions may change during processing. The logical extension of this is determining whether aFib amino terminal dimerization and aFib/Nop5p heterodimerization can occur concurrently or are mutually exclusive. Using techniques similar to those presented in this work the oligomeric state of the aFib/Nop5p complex with wildtype and amino terminal mutant aFibs can be determined *in vitro*. This approach could then be applied to L7Ae and box C/D RNAs. These types of studies may explain how multi-box C/D sRNP complexes form. A parallel set of experiments would target the role of the protein-protein interactions within the box C/D sRNP during catalysis. Reconstitution and catalysis by archaeal box C/D sRNP complexes has been successfully carried out *in vitro* (Omer *et al*., 2002). By comparing methylation efficiency of wildtype and mutant sRNP particles we can resolve interactions that are necessary for methylation. For example, constructing and comparing substrate methylation by box C/D sRNP particles with wildtype aFib*Sac* to those containing the aFib*Sac*_N6n11 and aFib*Sac*_N6n56 amino terminal mutants will directly assess the role of these interactions in catalysis. Together with our knowledge of how these mutants affect the stoichiometry of the sRNP complex, we will be able to assign roles to individual domains. Alternative approaches to elucidating protein-protein and protein-

RNA contacts include the titration or crosslinking of individual box C/D associated proteins or protein-protein complexes with wildtype or truncated box C/D sRNAs. This will allow us to determine which regions of the guide RNA interact with various protein components. Comparison of crosslinking patterns of the box C/D sRNP protein components at different stages of its catalytic cycle and in the presence of different substrates will provide important insight into the potentially different conformations these complexes adopt. This series of experiments will significantly add to our current understanding of these essential complexes and may provide a model for other, similar sRNP particles. Ultimately, three-dimensional structures of several complete box C/D sRNP particles in the presence and absence of different substrates will provide the highest resolution model of the complex.

References Cited

Aittaleb, M., R. Rashid, Q. Chen, J.R. Palmer, C.J. Daniels, H. Li (2003) Structure and function of the core protein complex of box C/D. *Nature Structural Biology* **10**: 256-263

Aittaleb, M., T. Visone, M.O. Fenley, H. Li (2004) Structural and thermodynamic evidence for a stabilizing role of Nop5p in *S*-adenosyl-L-methionine binding to fibrillarin. *The Journal of Biological Chemistry* **279**: 41822-41829

Amiri, K.A. (1994) Fibrillarin-like proteins occur in the domain *Archaea*. *Journal of Bacteriology* **176**: 2124-2127

Armbruster, D.W. & C.J. Daniels (1997) Splicing of Intron-containing tRNATrp by the archaeon *Haloferax volcanii* occurs independent of mature tRNA structure. *The Journal of Biological Chemistry* **272**: 19758-19762

Armstrong, D.J. & A. Roman (1993). The anomalous electrophoretic behavior of the human papillomavirus type 16 E7 protein is due to the high content of acidic amino acid residues. *Biochemical and Biophysical. Research. Communications* **192**: 1380–1387

Beattie T.L., W. Zhou, M.O. Robinson, L. Harrington (2001) Functional multimerization of the human telomerase reverse transcriptase. *Molecular and Cellular Biology* **21**: 6151-6160

Beaudette, N.V., & N. Langerman (1978) An improved method for obtaining thermal titration curves using micromolar quantities of protein. *Analytical Biochemistry* **90**: 693-707

Bernal, J.D. & D. Crowfoot (1934) X-ray photographs of crystalline pepsin. *Nature* **133**: 794-795

Bradford, M.M. (1976) A rapid and sensitive method for the quantitation of microgram

quantities of protein utilizing the principle of protein-dye binding. *Analytical Biochemistry* **72**: 248-254

Billings, P.C., J.W. Orf, D.K. Palmer, D.A. Talmage, C.G. Pan, M. Blumenfeld (1979) Anomalous electrophoretic mobility of *Drosophila* phosphorylated H1 histone: Is it related to the compaction of satellite DNA into heterochromatin? *Nucleic Acids Research* **6**: 2151–2164

Cahill, N.M, K. Friend, W. Speckmann, Z.H. Li, R.M. Terns, M.P. Terns, J.A. Steitz (2002) Site-specific cross-linking analysis reveal an asymmetric protein distribution for a box C/D snoRNP. *The European Molecular Biology Organization Journal* **21**: 3816-3828

Cavaille, J. & J.P. Bachellerie (1998) SnoRNA-guided ribose methylation of rRNA: structural features of the guide RNA duplex influencing the extent of the reaction. *Nucleic Acids Research* **26**: 1576-1587

Chothia, C. & J. Janin (1975) Principles of protein-protein recognition. *Nature* **256**: 705-708

Chothia, C. & A.M. Lesk (1986) The relation between the divergence of sequence and structure in proteins. *The European Molecular Biology Organization Journal*. **5**: 823-826

Clouet-d'Orval, B., M.L. Bortolin, C. Gaspin, J.P. Bachellerie (2001) Box C/D RNA guides for the ribose methylation of archaeal tRNAs. The tRNATrp intron guides the formation of two ribose-methylated nucleosides in the mature tRNATrp. *Nucleic Acids Research* **29**: 4518-4529

Clouet-d'Orval B., C. Gaspin, A. Mougin (2005) Two different mechanisms for tRNA ribose methylation in Archaea: a short survey. *Biochimie* **87**: 889-895

Collaborative Computational Project, Number 4 (1994) The CCP4 Suite: Programs for Protein Crystallography. *Acta Crystallographica D* **50**: 760-763

David, E., J.B. McNeil, V. Basile, R.E. Pearlman (1997) An unusual fibrillarin gene and

protein: structure and functional implications. *Molecular Biology of the Cell* **8**: 1051-1061

Davis, D.R., C.A. Veltri, L. Nielsen (1998) An RNA model system for investigation of pseudouridine stabilization of the codon-anticodon interaction in tRNALys, tRNAHis and tRNATyr. *Journal of Biomolecular Structure and Dynamics* **15**: 1121-1132

Deng, L., N.G. Starostina, Z.J. Liu, J.P. Rose, R.M. Terns, M.P. Terns, B.C. Wang (2004) Structure determination of fibrillarin from the hyperthermophilic archaeon *Pyrococcus furiosus*. *Biochemical and Biophysical Research Communications*. **315**: 726-732

Eddy, S.R. (2001) Non-coding RNA genes and the modern RNA world. *Nature Reviews. Genetics* **2**: 919-929

Eichler, E.C. & N. Craig (1994) Processing of eukaryotic ribosomal RNA. *Progress in Nucleic Acid Research and Molecular Biology* **49**: 197-239

Erdmann V.A., M.Z. Barciszewska, M. Szymanski, A. Hochberg, N. de Groot, J. Barciszewska (2001) The non-coding RNAs as riboregulators. *Nucleic Acids Research* **29**: 986-991

Ettinger, R.A., A.W. Liu, G.T. Nepom, W.W. Kwok (1998) Exceptional stability of the HLA-DQA1*0102/DQB1*0602 ab protein dimer, the class II MHC molecule associated with protection from insulin-dependent diabetes mellitus. *Journal of Immunology* **161**: 6439-6445

Fatica A. & D. Tollervey (2003) Insights into the structure and function of a guide RNP. *Nature Structural Biology* **10**: 237-239

Filipowicz W. (2000) Imprinted expression of small nucleolar RNAs in brain: Time for RNomics. *The Proceedings of the National Academy of Sciences of the United States of America* **97**: 14035-14037

Fournier, M.J. & E.S. Maxwell (1993) The nucleolar snRNAs: catching up with the

spliceosomal snRNAs. *Trends in Biochemical Sciences* **18**: 131-135

Ganot, P., B.E. Jady, M.L. Bortolin, X. Darzacq, T. Kiss (1999) Nucleolar factor direct the 2'-O-ribose methylation and pseudouridylation of U6 spliceosomal RNA. *Molecular and Cellular Biology* **19**: 6906-6917

Garcia de la Torre, J., M.L. Huertas, B. Carrasco (2000) Calculation of hydrodynamic properties of globular proteins from their atomic-level structure. *Biophysical Journal* **78**: 719-730

Gaspin, C., J. Cavaille, G. Erauso, J.P. Bachellerie (2000) Archaeal homologs of eukaryotic methylation guide small nucleolar RNAs: lessons from the *Pyrococcus* genomes. *Journal of Molecular Biology* **297**: 895-906

Gasteiger, E., C. Hoogland, A. Gattiker, S. Duvaud, M.R. Wilkins, R.D. Appel, A. Bairoch (2005) Protein identification and analysis tools on the ExPASy server. In Walker, J.M. (ed.), *The Proteomics Protocols Handbook*. Humana Press, Totowa, NJ, pp. 571-607

Gentile, F., P. Amodeo, F. Febbraio, F. Picaro, A. Motta, S. Formisano, R. Nucci (2002) SDS-resistant active and thermostable dimers are obtained from the dissociation of homotetrameric β-glycosidase from hyperthermophile *Sulfolobus solfataricus* in SDS. *The Journal of Biological Chemistry* **277**: 44050-44060

Ghisolfi, L., G. Joseph, F. Amalric, M. Erard (1992) The glycine-rich domain of nucleolin has an unusual supersecondary structure responsible for its RNA-helix-destabilizing properties. *The Journal of Biological Chemistry* **267**: 2955-2959

Guex, N. & M.C. Peitsch (1997) SWISS-MODEL and the Swiss-PdbViewer: An environment for comparative protein modeling. *Electrophoresis*. **18**: 2714-2723

Heine, M.A., M.L. Rankin, P.J. DiMario (1993) The gly/arg-rich (GAR) domain of *Xenopus* nucleolin facilitates *in vitro* nucleic acid binding and *in vivo* nucleolar localization. *Molecular Biology of the Cell* **4**: 1189-1204

Hemsley, A., N. Arnheim, M.D. Toney, G. Cortopassi, D.J. Galas (1989) A simple

method for site-directed mutagenesis using the polymerase chain reaction. *Nucleic Acids Research* **17**: 6545-6551

Hersh, R. T. & H.K. Schachman (1955) Ultracentrifuge studies with a synthetic boundary cell. II. Differential sedimentation. *Journal of the American Chemical Society* **77**: 5228-5234

Hu, C.C. & S.A. Ghabrial (1995) The conserved, hydrophilic and arginine-rich N-terminal domain of cucumovirus coat proteins contributes to their anomalous electrophoretic mobilities in sodium dodecylsulfate-polyacrylamide gels. *Journal of Virological Methods* **55**: 367–379

Jurica M.S. & M.J. Moore (2003) Pre-mRNAs splicing: Awash in a sea of proteins. *Molecular Cell* **12**: 5-14

Kawai G., Y. Yamamoto, T. Kamimura, T. Masegi, M. Sekine, T. Hata, T. Iimori, T. Watanabe, T. Miyazawa, S. Yokoyama (1992) Conformational rigidity of specific pyrimidine residues in tRNA arises from posttranscriptional modifications that enhance steric interaction between the base and the 2'hydroxyl group. *Biochemistry* **31**: 1040-1046

Kegeles, G. (1972) Z-average sedimentation coefficient in reversibly self-aggregating systems. *Proceedings of the National Academy of Science of the United States of America* **69**: 2577-2579

Kiss, T., C. Marshallsay, W. Filipowicz (1992) 7-2/MRP RNAs in plant and mammalian cells association with higher order structures in the nucleolus. *The European Molecular Biological Organization Journal* **11**: 3737-3746

Kiss T. (2001) Small nucleolar RNA-guided post-transcriptional modification of cellular RNAs. *The European Molecular Biological Organization Journal* **20**: 3617-3622

Kiss-Laszlo, Z., Y. Henry, J.P. Bachellerie, M. Caizergues-Ferrer, T. Kiss (1996) Site-specific ribose methylation of preribosomal RNA: a novel function for small nucleolar RNAs. *Cell* **85**: 1077-1088

Klein, D.J., T.M. Schmeing, P.B. Moore, T.A. Steitz (2001) The kink-turn: a new RNA secondary structure motif. *The European Molecular Biological Organization Journal* **20**: 4214-4221

Kowalak J.A., J.J Dalluge, J.A. McCloskey, K.O Stetter (1994) The role of posttranscriptional modification in stabilization of transfer RNA from hyperthermophiles. *Biochemistry* **33**: 7869-7876

Kuhn, J.F., E.J. Tran, E.S. Maxwell (2002) Archaeal ribosomal protein L7 is a functional homolog of the eukaryotic 15.5kD/Snu13p snoRNP core protein. *Nucleic Acids Research* **30**: 931-941

LaDu, M.J., T.M. Pederson, D.E. Frail, C.A. Reardon, G.S. Getz, M.T. Falduto (1995) Purification of apoliloprotein E attenuates isoform-specific binding to β amyloid. *The Journal of Biological Chemistry* **270**: 9039-9042

Laemmli, U.K. (1970) Cleavage of structural proteins during the assembly of the head of bacteriophage T4. *Nature* **22**: 680-685

Lane, B.G., J, Ofengand, M.W. Gray (1995) Pseudouridine and O2'-methylated nucleosides. Significance of their selective occurrence in rRNA domains that function in ribosome-catalyzed synthesis of the peptide bonds in proteins. *Biochimie* **77**: 7-15

Laue, M.T. & W.F. Stafford III (1999) Modern applications of analytical ultracentrifugation. *Annual Review of Biophysics and Biomolecular Structure* **28**: 75-100

Laue, T.M., B.D. Shah, T.M. Ridgeway, S.L. Pelletier (1991) Computer-aided interpretation of analytical sedimentation data for proteins. In Harding, S.E., A.J. Rowe, J.C. Horton (eds), *Analytical Ultracentrifugation in Biochemistry and Polymer Science.* Royal Society of Chemistry, Cambridge, UK, pp. 90-125

Maden, B.E. (1990) The numerous modified nucleotides in eukaryotic ribosomal RNA. *Progress in Nucleic Acid Research and Molecular Biology* **39**: 241-303

Marciani, D.J. & J.D. Papamatheakis (1978) Anomalous behavior of the major avian myeloblastosis virus glycoprotein in the presence of sodium dodecyl sulfate. *Journal of Virology.* **26**: 825-827

Maughan, D.W., J.A. Henkin, J.O. Vigoreaux (2005) concentrations of glycolytic enzymes and other cytosolic proteins in the diffusible fraction of a vertebrate muscle proteome. *Molecular and Cellular Proteomics* **4**: 1541-1549

Moore, T., Y. Zhang, M.O. Fenley, H. Li (2004) Molecular basis of box C/D RNA-protein interactions: Cocrystal structure of Archaeal L7Ae and a box C/D RNA. *Structure* **12**: 807-818

Omer, A.D., T.M. Lowe, A.G. Russell, H. Ebhardt, S.R. Eddy, P.P. Dennis (2000) Homologs of small nucleolar RNAs in Archaea. *Science* **288**: 517-521

Omer, A.D., S. Ziesche, H. Ebhardt, P.P. Dennis (2002) *In vitro* reconstitution and activity of a C/D box methylation guide ribonucleoprotein complex. *Proceedings of the National Academy of Sciences of the United States of America* **99**: 5289-5294

Omer A.D., S. Ziesche, W.A. Decatur, M.J. Fournier, P.P. Dennis (2003) RNA-modifying machines in archaea. *Molecular Microbiology* **48**: 617-629

Parker, K.A. & J.A. Steitz (1987) Structural analysis of the human U3 ribonucleoprotein particle reveal a conserved sequence available for base paring with pre-rRNA. *Molecular and Cellular Biology* **7**: 2899-2913

Philo, J. (1997) An improved function for fitting sedimentation velocity data for low molecular weight solutes. *Biophysical Journal* **72**: 435-444

Rabhi, I., N. Guedel, I. Chouk, K. Zerria, M.R. Barbouche, K. Dellagi, D.M. Fathallah (2004) A novel, simple and rapid PCR-based site-directed mutagenesis method. *Molecular Biotechnology* **26**: 27-34

Rashid, R., M. Aittaleb, Q. Chen, K. Spiegel, B. Demeler, H. Li (2003) Functional requirement for symmetric assembly of archaeal box C/D small ribonucleoprotein particles. *Journal of Molecular Biology* **333**: 295-306

Reddy, R. & H. Busch (1988) Small nuclear RNAs: RNA sequences, structure, and modifications. In Birnstiel, M.L. (ed.), *Structure and Function of Major and Minor Small Nuclear Ribonucleoprotein Particles.* Springer, Berlin, Germany, pp. 1-37

Reisfeld, R.A., U.J. Lewis, D.E. Williams (1962) Disk electrophoresis of basic proteins and peptides on polyacrylamide gels. *Nature* **195**: 281-283

Rozhdestvensky, T.S., T.H. Tang, I.V. Tchirkova, J. Brosius, J.P. Bachellerie, A. Huttenhofer (2003) Binding of L7Ae protein to the K-turn of archaeal snoRNAs: a shared RNA binding motif for C/D and H/ACA box snoRNAs in Archaea. *Nucleic Acids Research* **31**: 869-877

Russell, A.G., Y. Watanabe, J.M. Charette, M.W. Gray (2005) Unusual features of fibrillarin cDNA and gene structure in *Euglena gracilis*: evolutionary conservation of core proteins and structural predictions of methylation-guide box C/D snoRNPs throughout the domain Eucarya. *Nucleic Acids Research* **33**: 2781-2791

Schachman, H. K. & W.F. Harrington (1954) Ultracentrifuge studies with a synthetic boundary cell. I. General applications. *Journal of Polymer Science* **12**: 379-390

Schwede, T., J. Kopp, N. Guex, M.C. Peitsch (2003) SWISS-MODEL: an automated protein homology-modeling server. *Nucleic Acids Research* **31**: 3381-3385

Schwede, T., A. Diemand, N. Guex, M.C. Peitsch (2000) Protein structure computing in the genomic era. *Research in Microbiology* **151**: 107-112

Sollner-Webb, B., K. Tyc, J. Steitz (1996) Ribosomal RNA processing in eukaryotes. In Zimmerman, R. & A. Dahlberg (eds.), *Ribosomal RNA: Structure, Evolution, Processing and Function in Protein Synthesis*. CRC Press, Boca Raton, FL, pp. 469-490

Suryadi, J., E.J. Tran, E.S. Maxwell, B.A. Brown II (2005) The crystal structure of the *Methanocaldococcus jannaschii* multifunctional L7Ae RNA-binding protein reveals an induced-fit interaction with the box C/D RNAs. *Biochemistry* **44**: 9657-9672

Szewczak, L.B., S.J. DeGregorio, S.A. Strobel, J.A. Steitz (2002) Exclusive interaction

of the 15.5 kD protein with the terminal C/D motif of a methylation guide snoRNP. *Chemistry and Biology* **9**: 1095-1107

Thompson, J.D., D.G. Higgins, and T.J. Gibson (1994) CLUSTALW: improving the sensitivity of progressive multiple sequence alignment through sequence weighting, positions-specific gap penalties and weight matrix choice. *Nucleic Acids Research* **22**: 4673-4680

Tran, E.J., X. Zhang, E.S. Maxwell (2003) Efficient RNA 2'-O- methylation requires juxtaposed and symmetrically assembled Archaeal box C/D and C'/D' RNPs. *The European Molecular Biology Organization Journal* **22**: 3930-3940

Tran, E., X. Zhang, L. Lackey, E.S. Maxwell (2005) Conserved spacing between the box C/D and C'/D' RNPs of the archaeal box C/D sRNP complex is required for efficient 2'-O-methylation of target RNAs. *RNA* **11**: 285-293

Tycowski, K.T., C.M. Smith, M.D. Shu, J.A. Steitz (1996) A small nucleolar RNA requirement for site-specific ribose methylation of rRNA in *Xenopus*. *Proceedings of the National Academy of Sciences of the United States of America* **93**: 14480-14485

Tycowski, K.T., Z.H. You, P.J. Graham, J.A. Steitz (1998), Modification of U6 spliceosomal RNA is guided by other small RNAs. *Molecular Cell* **2**: 629-638

van Raaij, M.J., A. Mitraki, G. Lavigne, S. Cusack (1999) A triple β-spiral in the adenovirus fiber shaft reveals a new structural motif for a fibrous protein. *Nature* **401**: 935-938

Voet, D, & J.G. Voet (2004) Nucleic acid structures. In Harris D. & P. Fitzgerald (eds.) *Biochemistry (3rd Edition)*. Wiley and Sons, Hoboken, NJ, pp. 1116-1117

Vriend, G. (1990) WHAT IF: A molecular modeling and drug design program. *Journal of Molecular Graphics and Modeling* **8**: 52-56

Wang, H., D. Boisvert, K.K. Kim, R. Kim, S.H. Kim (2000) Crystal structure of a fibrillarin homologue from *Methanococcus jannaschii*, a hyperthermophile, at 1.6 Å resolution. *The European Molecular Biology Organization Journal* **19**: 317-323

Warner, J.R. (1990) The nucleolus and ribosome formation. *Current Opinion in Cell Biology* **2**: 521-527

Wassarman, K.M., A., Zhang, G. Storz (1999) Small RNAs in *Escherichia coli*. *Trends in Microbiology* **7**: 37-45

Watkins, N.J., V. Segault, B. Charpentier, S. Nottrott, P. Fabrizio, A. Bachi, M. Wilm, M. Rosbash, C. Branlant, R. Luhrmann (2000) A common core RNP structure shared between the small nucleolar box C/D RNPs and the spliceosomal U4 snRNP. *Cell* **103**: 457-466

Watkins, N.J., A. Dickmanns, R. Luhrmann (2002) Conserved stem II of the box C/D motifs is essential for nucleolar localization and is required, along with the 15.5 protein for the hierarchical assembly of the box C/D snoRNP. *Molecular and Cellular Biology* **22**: 8342-8352

Ziesche, S.M., A.D. Omer, P.P Dennis (2004) RNA-guided nucleotide modification of ribosomal and non-ribosomal RNAs in Archaea. *Molecular Microbiology* **54**: 980-993